Can individually targeted and optimized multi-channel tDCS outperform standard bipolar tDCS in stimulating the primary somatosensory cortex?

Asad Khan [a, *], Marios Antonakakis [a], Sonja Suntrup-Krueger [b], Rebekka Lencer [c, d], Michael A. Nitsche [e], Walter Paulus [f, g], Joachim Groß [a, h], Carsten H. Wolters [a, h]

[a] Institute for Biomagnetism and Biosignalanalysis, University of Münster, Münster, Germany
[b] Department of Neurology, University Hospital Münster, Münster, Germany
[c] Institute for Translational Psychiatry, University of Münster, Münster, Germany
[d] Department of Psychiatry and Psychotherapy, University of Lübeck, Lübeck, Germany
[e] Leibniz Research Centre for Working Environment and Human Factors at TU Dortmund, Dortmund, Germany
[f] Department of Neurology, Ludwig Maximilians University, München, Germany
[g] Department of Clinical Neurophysiology, University Medical Center, Georg-August University, Göttingen, Germany
[h] Otto Creutzfeldt Center for Cognitive and Behavioral Neuroscience, University of Münster, 48149 Münster, Germany

ARTICLE INFO

ABSTRACT

Background: Transcranial direct current stimulation (tDCS) has emerged as a non-invasive neuro-modulation technique. Most studies show that anodal tDCS increases cortical excitability, however, with variable outcomes. Previously, we have shown in computer simulations that our multi-channel tDCS (mc-tDCS) approach, the distributed constrained maximum intensity (D-CMI) method can potentially lead to better controlled tDCS results due to the improved directionality of the injected current at the target side for individually optimized D-CMI montages.
Objective: In this study, we test the application of the D-CMI approach in an experimental study to stimulate the somatosensory P20/N20 target source in Brodmann area 3b and compare it with standard bipolar tDCS and sham conditions.
Methods: We applied anodal D-CMI, the standard bipolar and D-CMI based Sham tDCS for 10 min to target the 20 ms post-stimulus somatosensory P20/N20 target brain source in Brodmann area 3b reconstructed using combined magnetoencephalography (MEG) and electroencephalography (EEG) source analysis in realistic head models with calibrated skull conductivity in a group-study with 13 subjects. Finger-stimulated somatosensory evoked fields (SEF) were recorded and the component at 20 ms post-stimulus (M20) was analyzed before and after the application of the three tDCS conditions in order to read out the stimulation effect on Brodmann area 3b.
Results: Analysis of the finger stimulated SEF M20 peak before (baseline) and after tDCS shows a significant increase in source amplitude in Brodmann area 3b for D-CMI (6—16 min after tDCS), while no significant effects are found for standard bipolar (6—16 min after tDCS) and sham (6—16 min after tDCS) stimulation conditions. For the later time courses (16—26 and 27—37 min post-stimulation), we found a significant decrease in M20 peak source amplitude for standard bipolar and sham tDCS, while there was no effect for D-CMI.
Conclusion: Our results indicate that targeted and optimized, and thereby highly individualized, mc-tDCS can outperform standard bipolar stimulation and lead to better control over stimulation outcomes with, however, a considerable amount of additional work compared to standard bipolar tDCS.

* Corresponding author. Student Institute for Biomagnetism and Biosignalanalysis, University of Münster Malmedyweg 15, 48149, Münster, Germany.
E-mail address: khana@uni-muenster.de (A. Khan).

1. Introduction

Transcranial direct current stimulation (tDCS) is a non-invasive brain stimulation technique to modulate cortical excitability by applying weak currents on the scalp conventionally with ≤ 2 mA through a pair of two large patch-like sponge electrodes ($25-35$ cm^2). The applied currents can induce excitatory or inhibitory modulation of cortical areas depending on the polarity, positive (anode) or negative (cathode), of the currents on the electrodes [1—4]. In sensorimotor applications [5—11], for anodal tDCS, an anodal patch electrode is placed over the primary motor (M1) or somatosensory cortex (S1) and a cathodal patch electrode over the supraorbital area, contra- (anode) and ipsilateral (cathode) to the side of stimulation, respectively. Anodal tDCS results in an excitability enhancement through membrane depolarization whereas cathodal tDCS results in excitability reduction via membrane hyperpolarization of the cortical neurons near the anode or cathode, respectively **[8, 9]**.

The sources for the early ($20-40$ ms) somatosensory evoked potentials (SEPs) in electroencephalography (EEG) and fields (SEFs) in magnetoencephalography (MEG), the cortical responses to the median nerve or finger stimulation, are generally accepted to have strong contributions from the primary sensorimotor cortex S1 contralateral to the side of stimulation [12—14]. The effect of tDCS on these early and late components were studied in Refs. [5—7,11] showing inhibitory or excitatory effects depending on stimulation parameters. For example, It was reported in Ref. [7] that a significant increase (excitatory effect) in amplitudes for the SEP peak-to-peak activities P25/N33, N33/P40 (parietal) and P22/N30 (frontal) after anodal tDCS was applied over the left motor cortex (M1), while no effect was observed for P14/N20, N20/P25 (parietal) and N18/P22 (frontal). Cathodal tDCS showed no effect on the SEP waveforms in their study. In Ref. [5], anodal tDCS over the S1 showed no effect on the N20 and N30 SEP components while a significant decrease (inhibitory effect) with cathodal tDCS was observed for the N20 SEP component. In Ref. [6], early N20 and P25 SEP components were significantly increased after anodal tDCS was applied over motor association cortex while opposite effects were observed after cathodal tDCS. In Ref. [11], where MEG was used to record SEF before and after applying tDCS, anodal tDCS was applied over M1 and S1 separately resulting in an increased effect for P35 and P60 SEF components for M1 and for the P60 SEF component for S1.

We summarize that the effect of tDCS on the SEP and SEF components in the above-mentioned studies showed inconsistencies. Differences in anodal electrode positions (M1, S1 and motor association cortex) and sizes (1.5 cm,^{2} 9 cm,^{2} 18 cm^2) might be a contributing factor to these inconsistent effects. More importantly when targeting a particular area, which in our study at hand is the generator for the P20/N20 SEF and SEP component in Brodmann area 3b, stimulating this brain region with only a standard bipolar montage, as studied by Refs. [8,9], might thus be too unspecific or even an inefficient approach [15]. The traditional bipolar tDCS approach broadly distributes electric fields in the brain which might lead to stimulation of non-target regions and diffused stimulation in the target brain area [16].

In this study, our goal is to use tDCS to stimulate a component that is as focal as possible and can be stably reconstructed, and in a second step targeted with tDCS, over a group of healthy subjects. This is the somatosensory component 20 ms post-stimulus, the so-called P20/N20 in EEG and M20 in MEG literature, due to its exogenous nature and its good signal-to-noise ratio [13,22]. This

might be done by either stimulating the index finger or the medianus nerve at the wrist. On the one hand, medianus nerve stimulation was shown to achieve a higher SNR [22], but on the other hand it leads to a much higher level of sensation and as a consequence might lead to too many drop-out of subjects. We therefore use electric finger stimulation in our experiment.

It has been shown that the use of the traditional bipolar tDCS approach might lead to inconsistencies [17] and inter-subject variability [18—20] of stimulation results. One cause of variability might be the lack of consideration of an individualized (subject-wise) targeting of stimulation, and also to different conductive profiles of head tissues and anatomical and functional differences between subjects [18,21—25]. For efficient tDCS targeting, injected currents should not only be maximal in the targeted brain region of interest (ROI), but minimal in non-target regions and oriented parallel to the target vector orientation for the desired effects [18,26—31].

To address these issues, we recently proposed a ~~novel~~ multichannel tDCS (mc-tDCS) approach, the distributed constrained maximum intensity (D-CMI) method [27]. We showed by computer simulations that, in comparison to standard bipolar tDCS, D-CMI optimized mc-tDCS achieves higher directionality, i.e., higher current density strength parallel to the target orientation and a higher mean focality. In experimental work, the former might mean larger effect sizes and the latter reduced side effects. Finally, the larger distribution of surface currents by our D-CMI method was assumed to reduce skin sensations and thereby ease the use of sham conditioning. With regard to the importance of high target directionality, first simulation and experimental work already showed that this can increase effect sizes [18,26,28—30,32,33]. However, until now, our D-CMI approach was not yet evaluated in any experimental work.

In the present study, we focused on anodal stimulations to keep the number of measurement sessions to a reasonable limit for our subjects (here: 4 measurement sessions per subject, the first EEG/MEG/MRI for targeting (Session 1), followed by three MEG/tDCS/MEG stimulation sessions (Session 2, 3 and 4).

We for the first time evaluate our D-CMI mc-tDCS optimization approach [27] in an experiment and compare it with the standard bipolar anodal tDCS (SB) as well as sham tDCS (Sham). Our experiment uses a single blind experimental tDCS paradigm with three sessions (Session 2, 3 and 4). The study is divided into two parts, targeting and stimulation. In the targeting part, we reconstruct the underlying source of the P20/N20 component in Brodmann area 3b by combined EEG/MEG/MRI source analysis (Session 1). After reconstructing this target source individually for each subject, we optimize a personalized multi-channel tDCS (mc-tDCS) montage using D-CMI. In the stimulation part of our experiment, we then carry out three stimulation sessions (Session 2, 3 and 4) with the individually optimized anodal D-CMI mc-tDCS (D-CMI), standard bipolar anodal tDCS (SB) and sham stimulation (Sham) in an SEF/tDCS/SEF experiment (Session 2, 3 and 4). SEF elicited by electric right hand index finger stimulation are recorded before and after tDCS interventions in the three randomized tDCS sessions (Session 2, 3 and 4). The after effects for each tDCS condition are statistically analyzed and compared for the SEF component at 20 ms. Throughout the study, for differentiating between recording of the same 20 ms component for targeting (Session 1) and tDCS conditions (Sessions 2, 3 and 4), we refer to the 20 ms somatosensory component as P20/N20, when recorded with combined EEG/MEG (SEP/SEF) in session 1 (targeting) and as M20, when recorded with MEG alone (SEF) before and after the application of the three tDCS conditions in sessions 2, 3 and 4 (tDCS stimulations). This is due to the fact that in EEG, the 20 ms component has a potential peak frontally (P20) and a potential trough occipitally (N20), whereas in

---

^{2} SimBio: a generic environment for bio-numerical simulations www.simbio.de, www.mrt.uni-jena.de/simbio.

MEG (when using radial gradiometers), the topography is rotated by 90° (M20) (see Fig. 1(b)).

Our focus is on the analysis of this 20 ms S1 component because of its exogenous nature [13,14], good signal-to-noise ratio (SNR) in both EEG and MEG and its overall robustness [34,35] even in the extreme case of aneasthesia [36]. Our goal is to answer the questions if (1) individually optimized mc-tDCS targeting with D-CMI can provide better controlled stimulation effects compared to SB and if (2) D-CMI optimization eases sham conditioning due to its low skin sensations. Throughout this study we will refer to the three tDCS stimulation conditions (Session 2, 3 and 4) as only D-CMI, SB or Sham for simplicity.

2. Material and methods

2.1. Participants

Thirteen right handed healthy subjects (28 ± 9 years, 3 Females) participated in this study. The subjects had no history of psychiatric or neurological disorders. There was no recreational drug use or medication use among the participants. The participants had given written informed consent before the experiment. The institution's ethical review board (Ethik Kommission der Ärztekammer Westfalen-Lippe und der WWU) approved all experimental procedures on 2.02.2018 (Ref. No. 2014-156-f-S).

2.2. Data acquisition for source analysis

2.2.1. MRI data acquisition and registration

In order to generate a realistic head model for source analysis (targeting), a MAGNETOM Prisma 3.0 T (Release D13, Siemens Medical Solutions, Erlangen, Germany) was used to acquire 3D-T1-weighted (T1w), 3D-T2-weighted (T2w), and diffusion-weighted (Dw) MRI datasets. A fast gradient-echo pulse sequence (TFE) using water selective excitation to avoid fat shift (TR/TE/FW = 2300/3.51 ms/8°, inversion pre-pulse with TI = 1.1 s, cubic voxels of 1 mm edge length) for T1w scans acquisition and a turbo spin echo pulse sequence (TR/TE/FA = 3200/408 ms/90°, cubic voxels, 1 mm edge length) for T2w scans acquisition was used. An echo planar imaging sequence (TR/TE/FA = 9500/79 ms/90, cubic voxels, 1.89 mm edge length), with one volume with diffusion sensitivity b = 0 s/mm^2 (i.e., flat diffusion gradient) and 20 vol with b = 1000 s/mm^2 in different directions, equally distributed on a sphere, was used to obtain Dw scans. Susceptibility artifacts were corrected by measuring and utilizing an additional volume with another flat diffusion gradient, but with reversed spatial encoding gradients [37]. Gadolinium markers were placed at nasion, left and right preauricular points during T1w measurement for later landmark-based registration purposes. Fig. 1(a) shows the T1w, T2w and Dw MRI scans for one of our subjects.
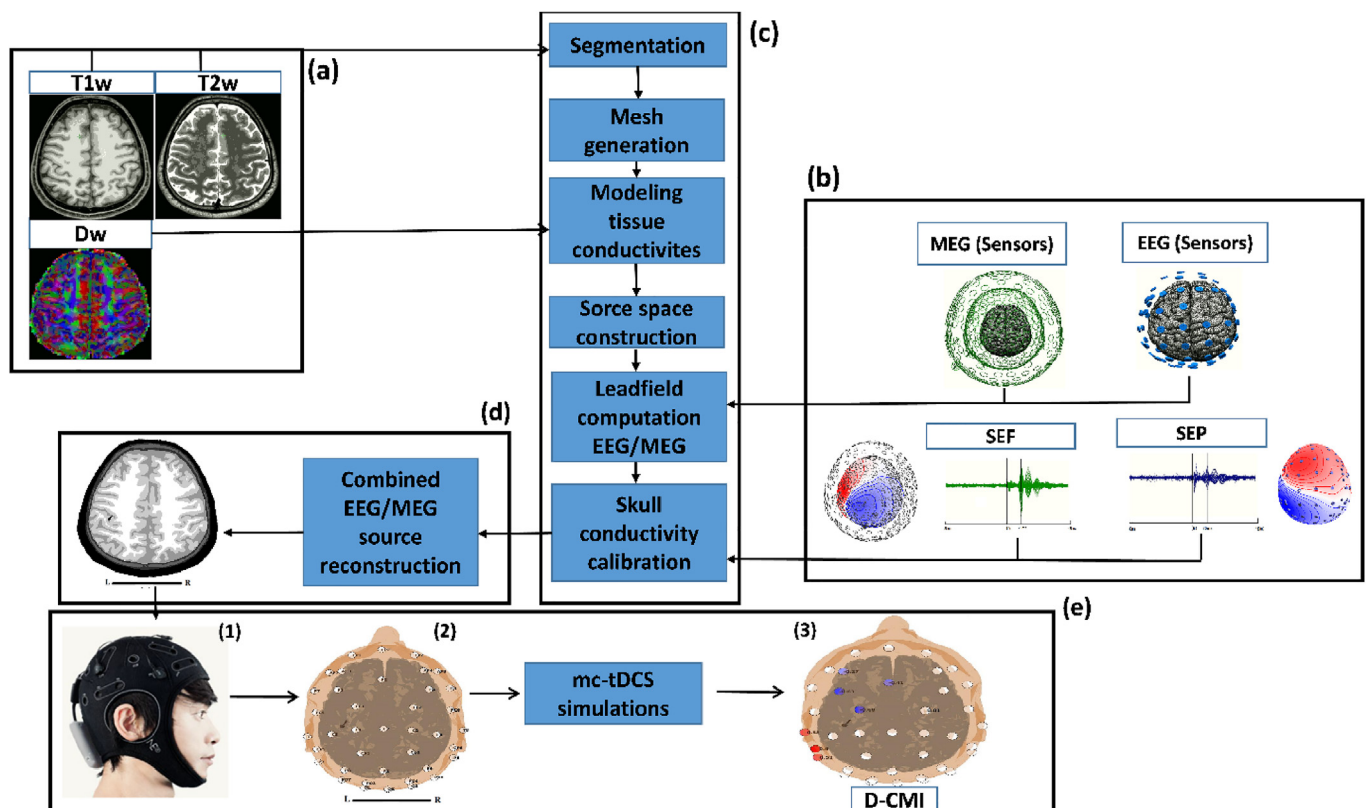

Fig. 1. Schematic diagram of the simulation pipeline for targeting in Session 1, i.e., reconstructing the P20/N20 activity by means of combined somatosensory evoked potentials (SEP) and fields (SEF) source analysis, and the following generation of tDCS stimulation montages. (a) Magnetic resonance imaging (MRI) data with T1w, T2w and Dw images acquired for modeling (b) Magnetoencephalography (MEG) and electroencephalography (EEG) registered sensor locations and SEF and SEP data sets and M20 and P20/N20 topographies (c) Forward modeling steps of segmentation, mesh generation, tissue conductivity modeling, source space construction, lead field computations for MEG and EEG and skull conductivity calibration. (d) Targeting by means of a P20/N20 dipole scan (black cone) visualized on the corresponding 6 compartment head model (e) tDCS montage generation steps where (e.1) shows a subject with the Starstim-8 system cap (e.2) the target source (Black dipole) and the registered and projected electrodes of the Starstim-8 cap on the head model (e.3) the individually targeted D-CMI optimized mc-tDCS montage.

2.2.2. Somatosensory evoked potential (SEP) and field (SEF) recordings and preprocessing

In order to reconstruct the underlying P20/N20 target, SEP and SEF were recorded simultaneously following electrical stimulation of the right hand index finger for 13 subjects. The simultaneous recording of MEG and EEG was carried out in a magnetically shielded room (Vacuumschmelze, Hanau, Germany). Throughout our whole experiment, EEG and MEG data were recorded in supine position to reduce head movements and to prevent distorting CSF-brain volume conduction effects due to the brain shift that would result from measuring EEG/MEG in a sitting position and MRI in a lying position [38]. The MEG system consisted of 275 axial gradiometers and 29 reference sensors (OMEGA 2005, VSM MedTech Ltd. Canada). Three magnetic coils were placed on nasion, left and right preauricular points to determine the subject's head position in relation to the MEG helmet. The EEG system consisted of 80 AgCl ring electrodes (EASYCAP GmbH, Hersching, Germany, 74 EEG electrodes plus additional six electrodes to detect eye movements). Before the measurement, the electrode positions of the EEG cap were digitized using a Polhemus device (FASTRAK, Polhemus Incorporated, Colchester, VT).

The electric stimuli were generated by a dual channel square pulse stimulator (Grass Instrument Division, Astro-Med, Inc., West Warwick, USA). Cup electrodes were applied on the right index finger with the cathode to the distal and anode to the proximal phalanx. A conductive gel was applied to the electrodes (Signa gel, Parker Laboratories, Inc., USA). Stimulation was done using a 0.2 ms pulse width with 3 times the sensitivity threshold. The inter-stimulus interval was varied randomly between 350 ms and 450 ms to avoid habituation. A recording of 40 min in blocks of 10 min was conducted with an online low pass filtering of 300 Hz and sampling rate of 1200 Hz. The finger stimulation-elicited combined SEP/SEF data was pre-processed with CURRY8, using bandpass filtering between 20 Hz and 250 Hz, notch filtering of 50 Hz (power line noise), and deselection of bad channels by visual inspection [13]. Trials with 50 ms pre-stimulus and 150 ms post-stimulus, overall of 200 ms lengths, were selected. Due to the randomization to avoid habituation, a 10 min run resulted in approximately 1200 trials. Bad trials were rejected using a threshold-based semi-automatic procedure offered in CURRY8 followed by visual inspection of the candidate bad trials in each modality. After this pre-processing, we averaged the remaining approximately 1100 ± 48 (mean ± SD) trials of each 10 min run to generate the SEP/SEF responses.

Our experience is that due to the overall large number of trials, even larger differences in the numbers of trials in the averages of the runs did not change the signal strengths of the 20 ms post-stimulus peaks, while the noise was reduced and the resulting signal-to-noise ratio (SNR) increased by the square-root of the number of trials in the average.

Fig. 1(b) shows for one of our subjects the EEG and MEG sensors over the registered cortex (top row) as well as the SEP and SEF butterfly plots and P20/N20 topographies (bottom row).

2.3. Source analysis and tDCS montage optimization

In order to compute individually optimized mc-tDCS montages for our somatosensory experiment, it was important to accurately reconstruct the underlying target source of the P20/N20 S1 component for each subject. This was done by, in our targeting session, means of combined EEG/MEG source analysis using the complementary information from the simultaneously measured SEP and SEF data. While MEG is a strong modality with regard to determining source location (much less influenced than EEG by individual conductivity parameters), MEG alone is not able to

determine source orientation accordingly due to the fact that it is nearly blind to radial sources. In a multi-layer sphere head model, an analytical formula can be derived for the MEG forward problem, which has no conductivity parameters and where radial source components do not produce any magnetic field outside the volume conductor [39]. In a realistic head model, regularization would thus be needed to avoid that spatially high-frequent noise components are amplified into unrealistically large radial source orientation components and thus unrealistically large source strengths [40]. The best stabilization to compensate for this limitation of MEG alone is thus to simultaneously analyse EEG and MEG [21,41,42]. However, due to the large inter- and intra-subject variability in skull conductivity [21] and the high sensitivity of EEG source analysis to the skull tissue parameters [39], we did not only build realistic subject-specific head volume conductor models, but also calibrated each head model for individual skull conductivity. However, due to the large inter- and intra-subject variability in skull conductivity [21] and the high sensitivity of EEG source analysis to the skull tissue parameters [43], we did not only build realistic subject-specific head volume conductor models, but also calibrated each head model for skull conductivity, as briefly described in the following.

2.3.1. Targeting using combined SEP/SEF source analysis in skull-conductivity calibrated realistic head models

Segmentation: We used T1w and T2w MRIs to build a six compartment head model of each subject representing the tissues scalp, skull compacta (SC), skull spongiosa (SS), cerebrospinal fluid (CSF), gray matter (GM), and white matter (WM). The segmentation process can be summarized as first segmenting scalp, GM and WM using the T1w image. Then, we registered the T2w to the T1w image using FSL [44] resulting in the T2w_T1w image. In a next step, we segmented SC, SS, CSF, and brain tissues using the T2w_T1w image as described in detail in Ref. [22]. In the last step, the resulting segmented tissues from the T1w image (scalp, GM and WM) and T2w_T1w image (SC, SS, CSF, and brain) were combined to form a six compartment head model. The head model was also cut with sufficient distance below the skull to reduce the computational complexity without loss of accuracy [45]. Fig. 1(d) shows a generated six compartment head model for one of our subjects.

Mesh generation: Hexahedral finite element method (FEM) meshing of the segmented head model was carried out using SimBio-VGRID.[1] In order to mitigate the stair-case effects of a regular hexahedral mesh and to increase conformance with the real geometry, a node shift approach was used on compartment interfaces resulting in a 1 mm geometry adapted hexahedral FEM mesh. A node shift of 0.33 was used, ensuring that the interior angles at the element vertices were convex and the Jacobian determinant in the FEM computation remained positive. This approach reduces numerical errors as shown in Ref. [46].

Modeling tissue conductivities: The isotropic conductivity values for the different tissue compartments of the six compartment head model were set as 0.43 S/m for scalp [47], 1.79 S/m for CSF [48] and 0.33 S/m for GM [49]. Skull conductivity was calibrated individually, as described below. The conductivity of the WM tissue compartment was modelled as anisotropic using the Dw images, as described in more detail in Ref. [50].

Source space construction: A source space was constructed consisting of nodes at the center of the GM tissue compartment with 2 mm resolution and without restriction to source orientations (no normal-constraint). In order to avoid modelling errors, it is essential that all sources are located inside the GM and in

---

[1] http://vgrid.simbio.de/.

sufficient distance from the neighboring tissue compartments to fulfill the so-called Venant condition. The Venant condition states that for each source node the closest FE node should only belong to elements which are labeled as GM [43,51,52].

Leadfield computation: Leadfields were computed for both EEG and MEG using SimBio-NeuroFEM[2] for the final step in forward modeling. EEG and MEG leadfield bases [49] and an algebraic multigrid preconditioned conjugate gradient (AMG-CG) [55] solver, proven to be stable with regard to tissue conductivity inhomogeneity and anisotropy [54,55], were used to achieve high computational speed [53].

Skull conductivity calibration: The combined EEG/MEG reconstruction of the P20/N20 S1 component is interlinked with the calibration of skull conductivity. While skull conductivity has a large influence on the EEG forward problem [43] and might vary inter- and intra-individually for example due to age [21,43], it hardly influences the MEG forward problem [21]. Therefore, we calibrated for skull conductivity using an algorithm, which uses the complementary information provided by the measured P20/N20 SEP and SEF topographies and the strength of MEG to determine source location and of EEG to determine source orientation as well as to estimate individual skull conductivity [21,56]. In a first step, a dipole scan is used to reconstruct the source underlying the peak of the SEF 20 ms component (peak means just one time sample). Then, after fixing the MEG location, the EEG is used to determine the dipole orientation. Lastly, with the fixed location and orientation, the dipole amplitude is determined from the MEG and the Residual Variance (RV) of the SEP P20/N20 component is stored. Repeating this for different skull conductivities, the conductivity with the lowest RV, leading to the best fitting dipole for both SEP and SEF 20 ms peak topographies, is then defined as the individually calibrated skull conductivity. To avoid overfitting, we only calibrated for skull compacta (SC) conductivity, while keeping the ratio to skull spongiosa (SS) conductivity, i.e., SC:SS, fixed to 1:3.6 following the measurements of [57]. A further advantage of this approach is that in case of erroneous assumptions on scalp conductivity, the resulting skull conductivity parameter counter balances this effect, so that EEG source reconstructions using calibrated skull conductivity resulted in lower errors than when using the standard value [56].

Combined EEG/MEG source reconstruction: We reconstructed the P20/N20 S1 targets individually in each subject using the realistic and skull-conductivity calibrated FEM head models for EEG and MEG forward solutions and the SEP/SEF run with highest SNR from Section 2.2.2. Single dipole scans (also known as deviation-, goal function-, or residual variance scans) [49,58] were used to estimate the target sources at the peak of the measured combined SEP/SEF P20/N20 responses in Brodmann area 3b of S1.

Fig. 1(c) summarizes the generation procedure for the skull-conductivity calibrated six compartment head modeling procedure and Fig. 1(d) shows a reconstructed P20/N20 target source in Brodmann area 3b for one of our subjects.

2.3.2. Generation of tDCS montages

For our somatosensory tDCS experiment, two kinds of montages were created, namely the D-CMI (and Sham) [27] and the SB [1,7] montages. We used a Starstim-8 tDCS system (Neuroelectrics, Barcelona, Spain). For D-CMI (and Sham), we used π cm^2 Ag/AgCl geled electrodes (Starstim NG Pistim) placed into holes of a neoprene cap corresponding to the international 10/10 EEG system (see Figs. 1(e) and 2). For the SB condition, 5 cm × 7 cm rectangular 35 cm^2 patch-electrodes (see Fig. 2) soaked with saline solution were used (Neuroelectrics Sponstim).

For the creation of these montages and in order to conform with the real experimental conditions, we first digitized the 39 possible

stimulation electrodes of our Starstim tDCS system with a Polhemus device (FASTRAK, Polhemus Incorporated, Colchester, VT) for each subject.

For each subject, the locations of the digitized sensors were registered on the head model using landmark-based rigid registration based on the three fiducials nasion, left and right preauricular points, where Gadolinium markers had also been placed for MRI (see Section 2.2.2). tDCS FEM forward models were then computed for each subject using SimBio-NeuroFEM as described in detail in Ref. [25] and the realistic and skull-conductivity calibrated individual FEM head models.

In the next step, the individualized tDCS forward models were used by our D-CMI optimization method to find the optimal mc-tDCS montage that best fits our stimulation goal, i.e., targeting the reconstructed individual Brodmann area 3b with highest directionality and potentially reduced side effects and skin sensations [27]. Therein, directionality (DIR) is defined as the scalar product between the current density vector at the target side, resulting from the surface injection currents, and the target orientation vector, i.e., the orientation of the pyramidal cells that produce the individual P20/N20 component [27,31]. DIR is thus a measure of the strength of the injected current intensity at the target side in the direction of the target orientation. A further interesting measure we will also use here is parallelity in percent (PAR%) [27,31], measuring DIR normed by the overall intensity in the target area times 100. PAR% thus indicates in percent how much of the injected current intensity at the target side is parallel to the target orientation. Note that even if the D-CMI optimizer maximizes DIR and not PAR%, it is interesting to also observe PAR%.

The D-CMI method makes use of three parameters, S_{Total}, $S_{maxelec}$ and λ [27]. S_{Total} is the total injected current, which we chose here to be 2 mA. $S_{maxelec}$ is the maximum current allowed per electrode, chosen here as 1.5 mA, which was found to be overall the highest tolerated intensity for our subjects without feeling discomfort when using our Starstim-8 system. The λ parameter distributes the currents over multiple electrodes to reduce skin sensations, while keeping DIR nearly at the same high level. We chose λ in a way that 8 non-zero electrodes resulted due to the availability of electrodes in our Starstim-8 system. In summary, these three parameters are used to create individually optimized montages for each subject not only using individual head modeling, but especially also individual target location and orientation. Thus, for each subject an 8 electrode montage was created using the D-CMI method, as illustrated in Fig. 1(e.3) for one of our subjects (see Suppl. Fig.2 in supplementary material for all subjects).

For the SB montage modeling, two 5 cm × 7 cm sponge-like tDCS patches with thickness 4 mm and saline-fluid-like conductivity of 1.4 S/m were used [25,27]. Following the standard montage as used in Refs. [1,7] the patches were centered at the C3 (anode) and FP2 (cathode) electrode locations that were digitized on each subject's head model as described above and visualized in Fig. 2. In accordance with the D-CMI condition, we also used for SB a total injection current of 2 mA.

2.4. Experimental design

We conducted a single blind (subjects), randomized, sham-controlled crossover group study with 13 subjects to determine the effects of our individually targeted and optimized D-CMI mc-tDCS approach, compared to the SB as well as Sham mc-tDCS.

In Fig. 2, we show the experimental paradigm with the three stimulation conditions D-CMI (Fig. 2(a)) together with its stimulation waveform (Fig. 2(b)), SB (Fig. 2(c)) together with its stimulation waveform (Fig. 2(d)), and Sham (Fig. 2(e)) together with its
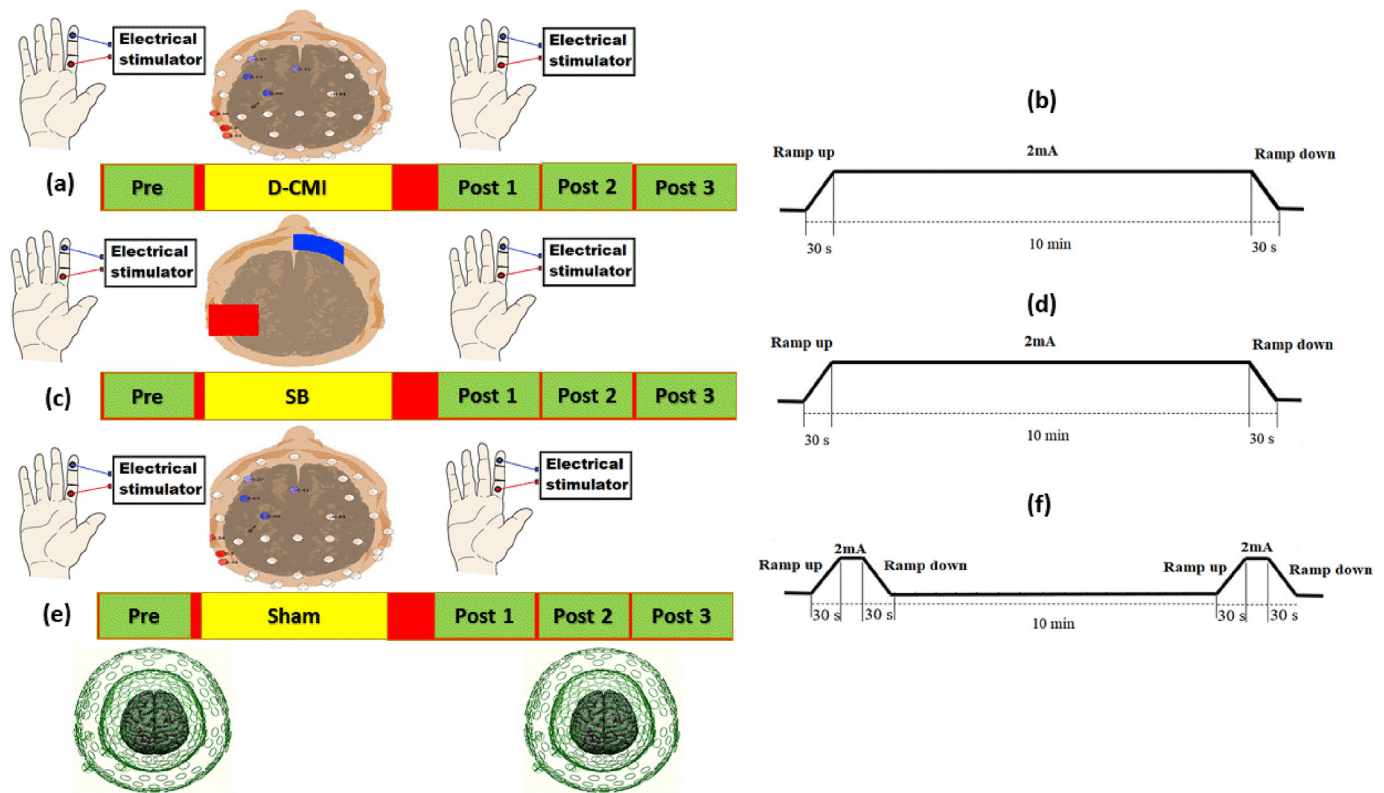
Fig. 2. Experimental design to stimulate the Brodmann area 3b in S1 with transcranial direct current stimulation (tDCS). MEG recording of somatosensory evoked fields (SEFs, green fields) before tDCS as Pre (10 min baseline) and after tDCS, with 5 min preparation time (red field), as Post1 (5–15min), Post2 (16–26 min), Post3 (27–37 min). The three different stimulation conditions are (a) distributed constrained maximum intensity (D-CMI) tDCS using (b) 30 s ramp up period, 10 min of 2 mA stimulation and ending with 30 s ramp down period, (c) standard bipolar tDCS (SB) using (d) 30 s ramp up period, 10 min of 2 mA stimulation and ending with 30s ramp down period, (e) D-CMI sham tDCS (sham) using (f) a 30 s ramp up to 2 mA immediately followed by 30 s ramp down period at the beginning and end of stimulation, and with 10 min with no stimulation in -between. (For interpretation of the references to colour in this figure legend, the reader is referred to the Web version of this article.)

stimulation waveform (Fig. 2(f)), exemplarily for one of our subjects.

In the tDCS experimental procedure, each subject's SEFs were recorded following right index finger stimulation (green fields in Fig. 2). Here, we used only MEG, because of (i) a considerable simplification and speed-up of the experimental setup, (ii) MEG's high sensitivity to source activity in Brodmann area 3b and (iii) the possibility to project the measured SEF data to the fixed Brodmann area 3b target sources from the targeting session (see Section 2.3). Like in the targeting session, the right index finger of each subject was stimulated with 3 times the sensitivity threshold at the beginning of each session.

The SEFs were recorded in a run of 10 min before tDCS (Pre) and three runs of 10 min after tDCS (Post1, Post2 and Post3) (green fields in Fig. 2). After tDCS, the heads of the subjects were briefly cleaned of electrode gel with a towel before re-entering the MEG shielded room (larger red fields in Fig. 2). Then, we first made sure that the index finger electrical stimulation intensity sensation was the same as in the Pre-tDCS SEF, before then measuring the three runs Post1, Post2 and Post3. All SEF's were recorded in supine positioning in accordance with Section 2.2.2 [38]. The parameters for recording of SEFs with the MEG system and post-processing were chosen as described in Section 2.2.2. Each subject participated in three tDCS conditions of 10 min each, namely D-CMI (upper row in Fig. 2), standard bipolar (SB, middle row in Fig. 2) and Sham (lower row in Fig. 2). Each tDCS stimulation condition was embedded in the 10 min SEF recording before (Pre: 10 min baseline) and the three 10 min SEF runs after tDCS, i.e., Post1 (5–15 min), Post2 (16–26 min) and Post3 (27–37 min). The

sessions were randomized and there was a break of minimally 6 days between the sessions to avoid any interference or carry over effect. In D-CMI and SB conditions, tDCS was applied for 10 min at 2 mA, preceded by a 30 s ramp-up period and followed by a 30 s ramp-down period at the end of stimulation (Fig. 2((b) and (d))). In the sham condition, tDCS was conducted by delivering the current for 30 s ramp-up and immediately 30 s ramp-down both at the beginning and the end of the 10 min period of no stimulation (Fig. 2(f)). The sham protocol was conducted in this way to induce the short-lasting tingling perceived during the transient period of current turn-on and -off like in the real stimulation conditions of D-CMI and SB.

All tDCS stimulation conditions were carried out with the Starstim-8 tDCS system (Neuroelectrics, Barcelona, Spain) as already explained in Section 2.3.2.

Questionnaires: After each stimulation session, subjects completed a self-report questionnaire to explore perceptions of adverse or side effects. The questionnaire contained rating scales for the presence and severity of side effects such as itching, pain, burning and warmth/heat sensations [1] on the scalp elicited by the three tDCS conditions (D-CMI, SB and Sham).

Following [1, Table 11], we used 4-point scales (0 = none, 1 = mild, 2 = moderate and 3 = strong) to rate the unpleasantness/uncomfortness of sensations on the scalp. For each condition, within the questionnaire subjects were asked to speculate whether they were receiving real or sham stimulation, to assess the integrity of subjects blinding using the 3-point rating scale (1 = real, 2 = placebo, 3 = I don't know) from [1, Table 11].

2.5. Data analysis

<u>Source space:</u> For the analysis of SEF's before and after tDCS interventions, the following steps were conducted.

(1) Computation of MEG lead fields (forward models) by performing the same procedure as in section 2.3.1 for each subject before and after each tDCS condition (D-CMI, SB and Sham) due to the possibly slightly different subject positioning in the MEG dewar.
(2) Computation of source waveforms for the M20 component by data projection, i.e., taking the scalar product of the MEG lead field of the individual dipole target (reconstructed from combined SEP/SEF as described in Section 2.3.1) with the measured SEF M20 component divided by the square of the L2-norm of the MEG lead field. Due to the complementarity of EEG and MEG, we thus fix the target source of the combined SEP/SEF reconstruction and project the SEF data of three stimulation conditions to this target source under the additional assumption that the expected change in excitability of S1 would not lead to a shift in source location and orientation. The source waveforms for the M20 are then stored for later analysis.
(3) In the last step we take the peak amplitudes (peak means just one time sample) of the M20 components of the source waveforms pre and post (Post1, Post2 and Post3) tDCS conditions (D-CMI, SB and Sham) for each subject.

After these three steps, statistical analysis was conducted for the M20 peak amplitudes of the source waveforms for time courses before (Pre) and after (Post1, Post2, Post3) tDCS conditions (D-CMI, SB and Sham).

In 2 of the 13 subjects (see Suppl. Fig. 1(a)–(c): subjects A2350 for all conditions Suppl. Fig. 1(a)–(c) and A1922 for D-CMI) a clear signal peak around 20 ms post-stimulus could not be detected in at least one SEF run, so that they were excluded from further analysis. Furthermore, one further subject was detected as outlier with regard to its M20 amplitude, exceeding 2 standard deviation from the mean (see Suppl. Fig. 1(a): subject A2263). The noise in these subjects limited the SNR of the M20 peak component, caused for example by possible finger or arm movements and resulting finger stimulation artifacts in the averaged SEF data, remaining head movements in the MEG dewar even in lying positioning due to fatigue and limited goodness-of-fit of the projected data to the fixed source location and orientation. Therefore, a remaining number of 10 subjects, same from each condition, are used for further within-subject group statistical analysis.

A within-subject two-way repeated measures analysis of variance (RM-ANOVA) was conducted for the 10 subjects for the analysis of interaction effects (conditions x time) among the conditions. Greenhouse-Geisser correction was used for non-sphericity wherever necessary. Post hoc paired sample t-tests with bootstrapping (1000 permutations) were then performed for multiple comparisons between control values (Pre) and those after tDCS (Post1, Post2 and Post3) for the three conditions (D-CMI, SB and Sham) separately. A P value of less than 0.05 was considered significant for all statistical analyses.

<u>Sensor space:</u> To complement the source space analysis in sensor space, we analyzed the M20 SEF component in the time range of 19—21 ms with a non-parametric cluster based permutation test [55] for Pre vs Post (Post1, Post2 and Post3) time course differences for all conditions (D-CMI, SB and Sham) separately. From a dependent paired *t*-test for time course comparisons all samples showing a t-value greater than a threshold corresponding to P = 0.05 (uncorrected) were selected and spatially clustered. The

level of the statistics of the cluster was defined as the sum of t-values within the cluster. The cluster with the maximum value was used to construct the statistics. A reference distribution of maximum cluster t-values was obtained by randomization of data across the time courses for each condition separately for 1000 times and was used to evaluate the statistics of the actual measured SEF data.

<u>Questionnaire data:</u> We analyzed the questionnaire data for perceived sensations (Itching, Pain, Burning and Warmth/heat) with a non-parametric Friedman ANOVA test for each sensation and each tDCS condition (DMCI, SB and Sham) separately. A p-value of less than 0.05 was taken as significant. We also analyzed the Sham perception questionnaire data with a Friedman ANOVA test.

We used SPSS[3] Statistics (V 28.0.1) for all statistical analysis and FieldTrip [59] for post processing of MEG data before and after tDCS interventions and cluster based permutation statistical analysis.

3. Results

3.1. Results of targeting and montage optimization

The investigations for sections 2.2 and 2.3 (Session 1) are carried out for all 13 subjects. We provide in Fig. 1(a) a schematic diagram of the simulation pipeline that leads to the creation of D-CMI (and Sham) tDCS montages for a P20/N20 S1 target for one of our subjects. In Fig. 1(a) (upper left) the acquired T1w-, T2w- and Dw-MRI data are shown which together with the measured SEP and SEF P20/N20 topographies (Fig. 1(b)) enable the generation (Fig. 1(c)) of an individual six-compartment head model (Fig. 1(d)) with calibrated skull conductivity and anisotropic white matter compartment. This head model served the EEG and MEG forward computations and enabled combined EEG/MEG inverse dipole scanning of the individual P20/N20 target (black cone in Fig. 1(d)). In a last step, the targeted (to this black cone) and individually optimized mc-tDCS montage was computed using our D-CMI approach [27] (Fig. 1(e.3)), which then also serves our Sham condition as shown in Fig. 2(c).

The skull conductivity calibration (Section 2.3.1 and Fig. 1(c)) resulted in individual skull conductivities for the 13 subjects with a mean and a standard deviation for skull compacta (SC) and skull spongiosa (SS) of 6.7 ± 5.12 mS/m and 24.1 ± 15.4 mS/m, respectively. In contrast to the strong personalization of the D-CMI approach, the only personalization aspect of the SB tDCS montage (Fig. 2(b)) was that the patches were centered at the C3 (anode) and FP2 (cathode) electrode locations that were determined and digitized individually based on each subject's head model using the Polhemus device.

While the bipolar montages are thus only standardized, the D-CMI mc-tDCS montages are largely personalized with regard to head modeling, determination of the target as well as optimization for maximal directionality with potentially reduced side effects and skin sensations. Fig. 3(a) shows how different the D-CMI montages can be, depending especially on individual target orientation differences. D-CMI montages (Fig. 3(a), left column) and EEG P20/N20 topographies are presented for three exemplary participants together with the D-CMI montages (Fig. 3(a), right column) to emphasize the importance of individualized montage calculation (Session 1). The results for all 13 subjects are presented in Suppl. Fig.2, which shows the individually optimized D-CMI mc-tDCS montages together with the target source dipoles (columns 1 and 4), the D-CMI montages visualized over the EEG P20/N20 topographies (columns 2 and 5) and the target source dipoles in the
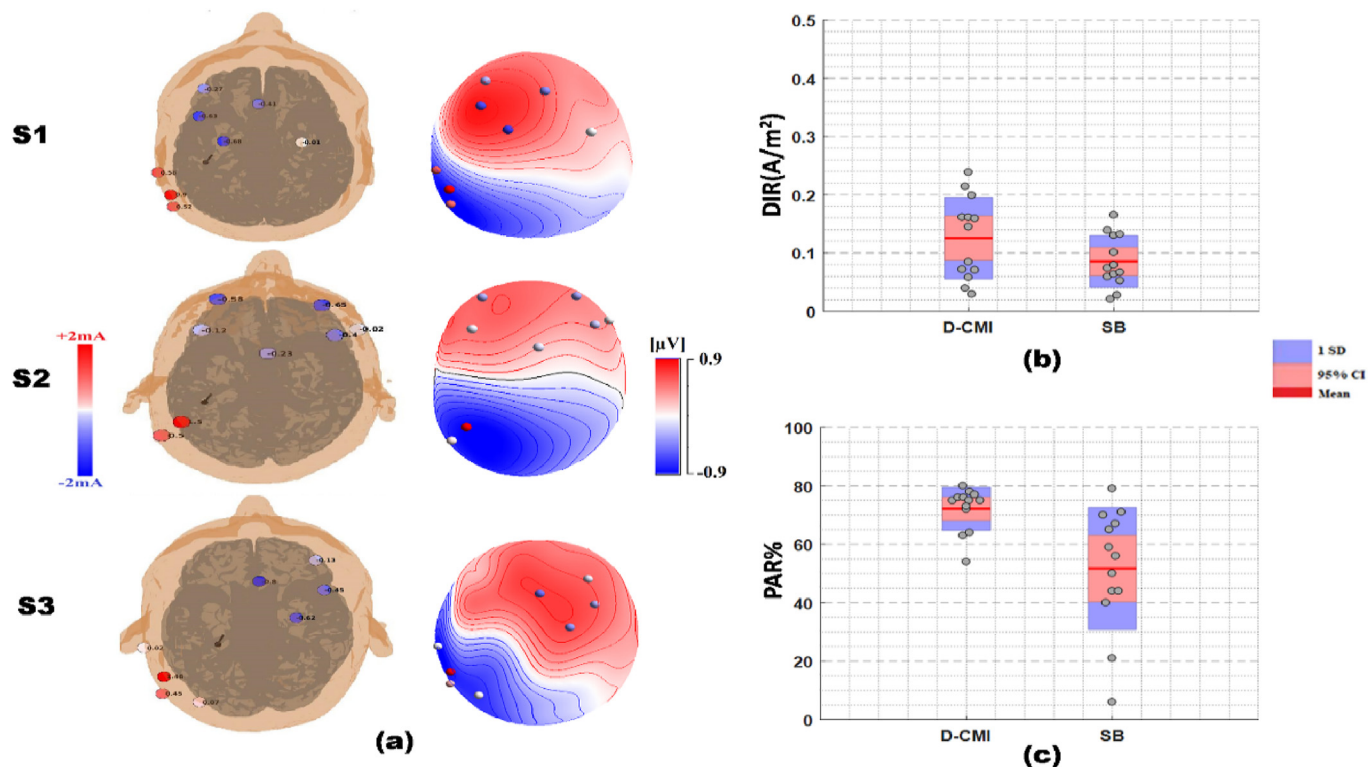

Fig. 3. The results for the D-CMI mc-tDCS method are shown as (a) D-CMI mc-tDCS montages together with target sources (column 1) and D-CMI montages visualized over the EEG P20/N20 topographies (column 2) exemplarily for three subjects (S1, S2 and S3) (b) directionality (DIR) (N = 13) and (c) parallelity in percent (PAR%) (N = 13) comparison of D-CMI and SB as boxplots with mean (red line), 95% confidence interval (95% CI) (pink) and 1 standard deviation (1 SD) (blue). (For interpretation of the references to colour in this figure legend, the reader is referred to the Web version of this article.)

anatomical T1-MRIs (columns 3 and 6). Fig. 3(b) presents the resulting DIR, as defined in Section 2.3.2, for our group of 13 subjects with a specialized boxplot[4] showing mean (red line), 95% confidence interval (95% CI) (pink) and 1 standard deviation (1 SD) (blue). The mean $\pm$ SD DIR for D-CMI (0.126 $\pm$ 0.070 A/m^2) and SB (0.085 $\pm$ 0.044 A/m^2) and a statistical comparison of DIR (D-CMI vs SB) with paired samples t-tests (bootstrapping 1000 permutations) shows that individually targeted D-CMI mc-tDCS potentially increases the chance for more controlled effects when compared to SB (P = 0.024). Furthermore in Fig. 3(c) we show PAR%, as also defined in Section 2.3.2. This parameter complements DIR and clearly shows that PAR% (mean $\pm$ SD) for D-CMI (72.15 $\pm$ 7.38%) is much higher than for SB (51.69 $\pm$ 20.87%). We can thus hypothesize from the computer simulation results that individually targeted and optimized D-CMI mc-tDCS might, due to its individually optimized DIR, reduce individual differences in effects when compared to SB, i.e., it might lead to more controlled tDCS effects.

3.2. Results of the tDCS stimulation experiment

The investigations for sections 2.4 and 2.5 (Sessions 2, 3 and 4) are carried out for the 10 subjects (N = 10), as described in section 2.5.

3.2.1. Source space results

In Fig. 4(a)–(c) we show the grand averaged (N = 10) source waveforms (0–30 ms) around the M20 SEF component with time courses, Pre (Blue), Post1 (Red dotted), Post2 (Green dotted) and

Post3 (Black dotted), for the three stimulation conditions D-CMI (Fig. 4(a)), SB (Fig. 4(b))) and Sham (Fig. 4(c)).

In Fig. 5, we show for the 10 subjects boxplots (upper row, showing the mean in red, 95% confidence interval in pink and 1 SD in blue) and complementary error bar plots (lower row, with means as red boxes and standard deviations as vertical blue line) for the grouped peak amplitudes of M20 source waveforms for each time course (Pre, Post1, Post2 and Post3) and each condition (D-CMI, SB and Sham) separately. Amplitudes of M20 source waveforms after tDCS, for time courses Post1, Post2 and Post3, are normalized to Pre tDCS M20 source waveform amplitudes as baseline normalization and shown individually in the upper row and as group averaged in the lower row of Fig. 5.

Table 1 shows the mean and standard deviation (Mean(SD)) of M20 (20 ms) source waveform amplitudes for the group of 10 subjects in each condition and time course. . In the supplementary material in Suppl. Fig. 1(a)–(c), source waveforms are shown for all 13 subjects and all three conditions. Table 2 shows the results of a two way within-subject RM-ANOVA for the interaction effect among the tDCS conditions for all time courses. Table 3 further shows for Table 2 the interaction effects among the tDCS conditions for Pre vs Post time courses between the conditions. Table 4 shows the post-hoc paired sample *t*-test results for Tables 2 and 3. Table 4 also shows the Cohen's d effect size for the time course compared to Pre baseline tDCS complementing the results for Table 3.

From the two way RM-ANOVA, as indicated in Table 2, an overall significant interaction effect is observed among the conditions for D-CMI vs SB vs Sham (P = 0.012*). A significant interaction effect is observed when separate comparisons were conducted for D-CMI vs SB (P < 0.001***) and D-CMI vs Sham (P = 0.045*). No significant interaction effect can be seen for SB vs Sham (P = 0.63) comparison.

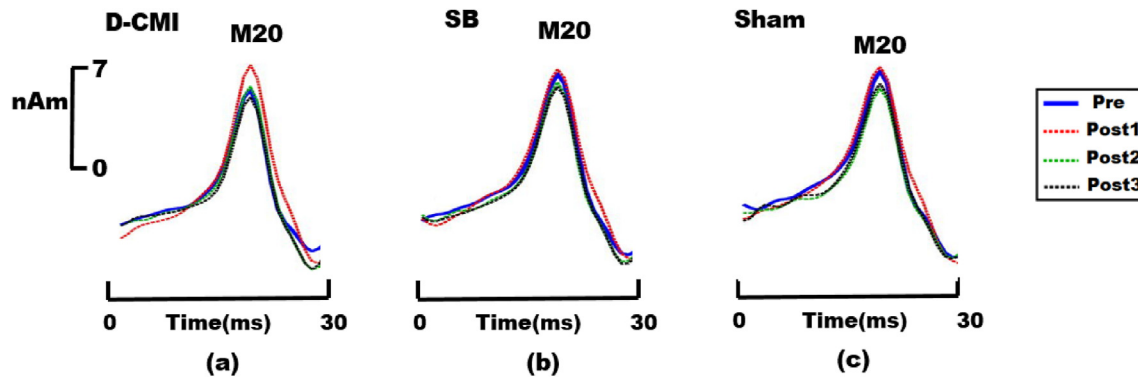[4] https://github.com/raacampbell/notBoxPlot.

Fig. 4. Grand averaged (over the 10 subjects) source waveforms around the M20 are shown for before tDCS as Pre (Blue) and after tDCS as Post1 (Red dotted), Post2 (Green dotted) and Post3 (Black dotted) when stimulated with (a) distributed constrained maximum intensity (D-CMI) mc-tDCS (b) standard bipolar tDCS (SB) and (c) D-CMI sham tDCS (Sham). (For interpretation of the references to colour in this figure legend, the reader is referred to the Web version of this article.)

With Table 3 results, the interaction effects can be observed at each time course comparison (Pre vs Post) between the conditions. It is observed from Table 3 that there is a significant difference between D-CMI vs SB for Pre vs Post1 (P < 0.001**) and D-CMI vs Sham for Pre vs Post1 (P = 0.009*) comparison.

For D-CMI, the post-hoc paired sample *t*-test in Table 4 reveals a significant main effect for Pre vs Post1 (P = 0.018*), non-significant effects for Pre vs Post2 (P = 0.516) and Pre vs Post3 (P = 0.49). Fig. 5 (first column) shows that the M20 amplitude for the D-CMI increased on average 27% in the first 5–15 min (Post1) after tDCS, while it increased by only 3% in Pre vs Post2 and decreased by 6% in the Pre vs Post3 time course comparison.

For the SB, post-hoc paired sample *t*-test, in Table 4, revealed non-significant effects for Pre vs Post1 (P = 0.51), Pre vs Post2 (P = 0.127) and Pre vs Post3 (P = 0.06). Fig. 5 (middle column) shows that the M20 amplitude for SB deceased on average 1% for Pre vs Post1, 12% for Pre vs Post2 and 16% for Pre vs Post3 time courses.

For the Sham, post-hoc paired sample *t*-test, in Table 4, showed a non-significant effect for Pre vs Post1 (P = 0.85) and Pre vs Post2 (P = 0.146) and a significant effect for Pre vs Post3 (P = 0.031*). The M20 amplitude change for Sham decreased on average 3% for Pre vs Post1, 16% for Pre vs Post2 and 18% for Pre vs Post3 time courses (see Fig. 5 third column).
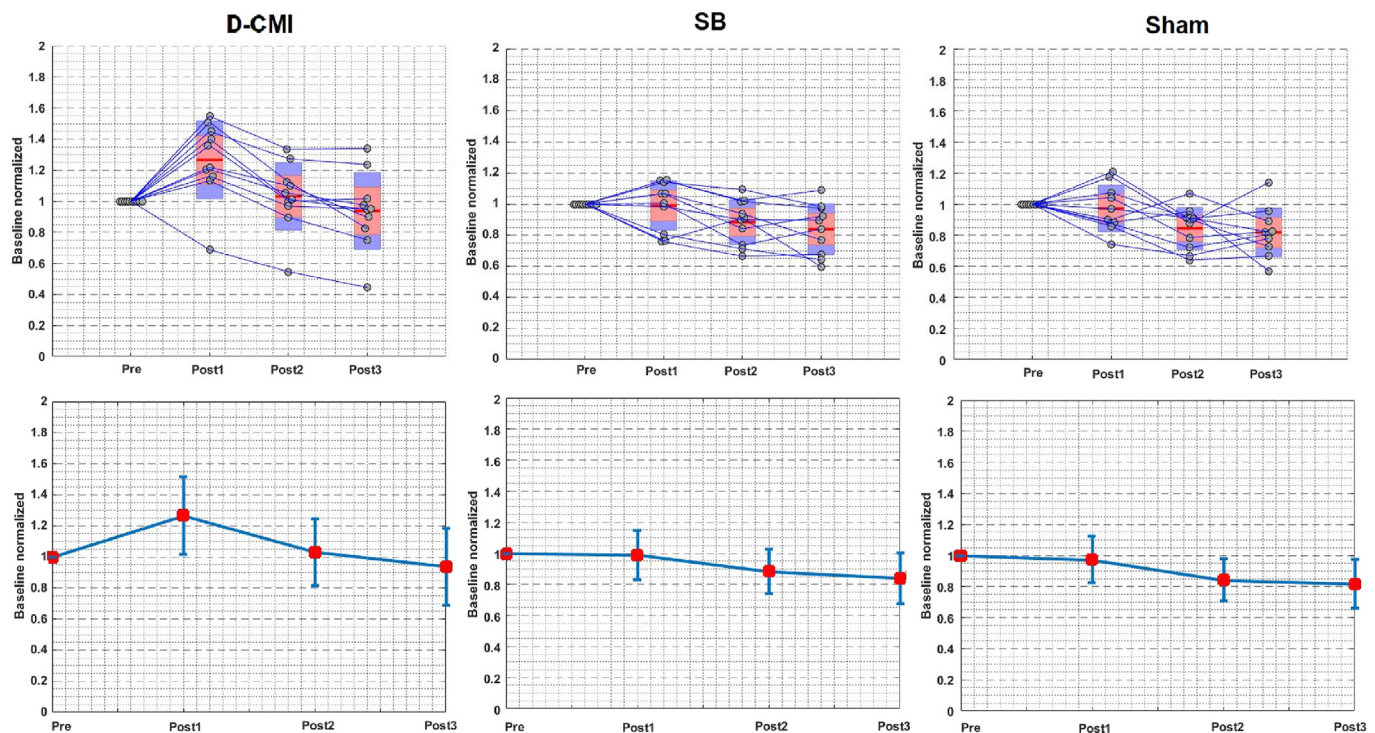

Fig. 5. N = 10: Baseline (Pre) and after-effects (Post1, Post2, Post3) of the three tDCS stimulation conditions distributed constrained maximum intensity (D-CMI) (left column), standard bipolar (SB) (middle column) and D-CMI sham (Sham) (right column) are shown with boxplots (upper row, showing the mean in red, 95% confidence interval in pink and 1 standard deviation in blue) and error bar plots (lower row, with means as red boxes and standard deviations as vertical blue lines). The M20 peak amplitudes of source waveforms for Post1, Post2 and Post3 are normalized to Pre tDCS M20 source waveform amplitudes and shown individually (upper row boxplots) for D-CMI, SB and Sham. (For interpretation of the references to colour in this figure legend, the reader is referred to the Web version of this article.)

Table 1

Mean and standard deviation (Mean(SD)) of the M20 source waveform peak amplitudes in nAm for the 10 subjects for Pre, Post1, Post2 and Post3 in the tDCS conditions of distributed constrained maximum intensity (D-CMI), standard bipolar (SB) and D-CMI sham (Sham) sessions.

Conditions	Mean(SD) in nAm			
	Pre	Post1	Post2	Post3
D-CMI	4.4(2.74)	5.54(3.62)	4.59 (3.15)	4.18(2.84)
SB	4.21(2.71)	4.36(3.23)	3.93(2.98)	3.78(3)
Sham	4.4(3.26)	4.46(3.83)	3.9(3.59)	3.73(2.85)

Regarding effect sizes in Table 4, only the D-CMI showed more than a very large effect size in the Pre vs Post1 comparison (d = 1.21), while all other effect sizes were only medium to large.

3.2.2. Sensor space results

In Fig. 6, we show the resultant t-value topographies for non-parametric cluster-based permutation tests for 10 subjects. We show the conditions in rows with Fig. 6(a) for D-CMI, Fig. 6(b) for standard bipolar (SB) and Fig. 6(c) for Sham, and time course comparisons to pre tDCS in columns for Pre vs Post1 (Column 1), Pre vs Post2 (Column 2) and Pre vs Post3 (Column 3). Fig. 6 complements Table 4 with a statistical *t*-test in sensor space for the measured SEF data before (Pre) and after (Post1, Post2 and Post3) tDCS.

In the sensor space analysis (Fig. 6), the non-parametric cluster-based permutation test showed similar results as the source space analysis in Table 4. For the D-CMI condition, significant clusters were observed for the Pre vs Post1 time course comparison with negative and positive clusters (Fig. 6(a.1)). No significant clusters were present for Pre vs Post2 (Fig. 6(a.2)) and Post3 (Fig. 6(a.3)) time course comparisons. In the SB session, no significant negative or positive clusters were observed in the Pre vs Post1 (Fig. 6(b.1)) and Pre vs Post2 (Fig. 6(b.2)) conditions and Pre vs Post3 (Fig. 6(b.3)) time course comparison. In the Sham condition, significant positive and negative clusters were observed for only the Pre vs Post3 (Fig. 6(c.3)), and no significant clusters were observed for the Pre v Post1 (Fig. 6(c.1)) and Post2 (Fig. 6(c.2)) time course comparisons.

<u>Questionnaire results</u>: In Table 5, for all 13 subjects, we show the results of the non-parametric Friedman test applied on the perceived sensation data for each condition separately. In Table 6 we show the results of the non-parametric Friedman test applied on the sham perception data. All subjects tolerated the application of the currents in the different conditions well and there was no disruption of the experimental procedures due to adverse or side effects.

Table 5 summarizes the mean intensity of the sensations according to the questionnaire for scaled sensations (itching, pain, burning and warmth/heat) over the scalp induced by tDCS (D-CMI, SB and Sham). The non-parametric Friedman ANOVA test for each

Table 2

Results of a two way with-subject repeated measures ANOVA (RM-ANOVA) for the 10 subjects showing the interaction effect between the tDCS conditions for all time courses (Pre, Post1, Post2 and Post3). Statistical results are shown when conditions are compared, with degrees of freedom (df), F values (F) and P-values (P) (*P < 0.05, **P < 0.01, ***P < 0.001).

Conditions comparison	Interaction effect (Condition x Time) df, F, P, Error(df)
D-CMI vs SB vs Sham	6,3.067, **0.012***, 54
D-CMI vs SB	3, 7.84, < **.001*****, 27
D-CMI vs Sham	3, 3.07, **0.045***, 27
SB vs Sham	3, 0.585, 0.63, 27

sensation between conditions did not result in any significant group difference between conditions. No significant differences in the intensity of perceived sensations of itching ($\chi^2(2) = 3.16$, P = 0.21), pain ($\chi^2(2) = 4.46$, P = 0.11), burning ($\chi^2(2) = 4.33$, P = 0.12) and warmth/heat ($\chi^2(2) = 3.25$, P = 0.19) was observed. The non-parametric Friedman ANOVA test resulted in no significant differences for the guesses about Sham or real stimulations of D-CMI and SB ($\chi^2(2) = 4.46$, P = 0.11). Table 5 summarizes the guesses about the stimulation conditions.

Table 6 shows that 10 subjects considered both D-CMI and Sham to be real stimulations, while 3 subjects were unsure. SB was the only condition rated as sham by a larger subgroup (6 times as Sham and 7 times as real). From these observations it can be concluded that the majority of the subjects in the conditions perceived tDCS in all conditions as a real stimulation and were unable to detect a Sham stimulation accurately.

4. Discussion

In the present study, we for the first time examined the effects of the individually targeted and D-CMI optimized mc-tDCS approach [27] in a brain stimulation experiment. We used a well-controlled somatosensory setup in a group of 13 healthy subjects. Our target area was the underlying source of the SEP and SEF P20/N20 component in Brodmann area 3b (S1), elicited by electrical stimulation of the right index finger. Individual targeting was performed by means of source analysis of the P20/N20 component, using the complementary information of combined SEP/SEF data. Source analysis used individual skull-conductivity-calibrated six compartment anisotropic FEM head models of the subjects. In the targeting, the strength of MEG was used to determine the source location, while additional EEG data were used for determination of the source moment (i.e., source orientation and strength) as well as for estimation of individual skull conductivity. The generated subject-specific FEM head models were then also used for tDCS forward simulations and optimization of D-CMI electrode montages. Experimental effects of (i) the individually targeted and optimized D-CMI mc-tDCS, (ii) SB tDCS and (iii) D-CMI-based sham stimulation were then compared. Since we used anodal D-CMI and SB stimulations, an excitatory effect was expected when compared to Sham. While [7] and [5] used EEG, we used MEG as also measured in Ref. [11] to determine stimulation effects on the ~~P20/N20 (or M20~~ target source in Brodmann area 3b, due to the higher sensitivity of MEG to the lateral and mainly tangential activity of Brodmann area 3b [14,22,60]. Therefore, we projected the SEF measurements pre- and post- tDCS to the fixed source locations and orientations from the EEG/MEG targeting process (Session 1), because due to the use of the complementary information in EEG and MEG we expect a more stable Brodmann area 3b reconstruction from the simultaneous SEP/SEF source analysis [49,61,62].

We show that inter-individual differences of the P20/N20 source can not only be found in target location, but especially also in orientation (Fig. 3(a)). As also shown by others [18,26,28−30,32,33], orientation might play an especially important role in individualized targeting. We furthermore demonstrated that the resulting targeted and D-CMI optimized mc-tDCS montages show considerable inter-individual differences (Fig. 3(a−c)). Our FEM-based computer simulations show that the individual D-CMI mc-tDCS montages, when compared to SB, lead to significantly increased current directionality (DIR) at the target side. Furthermore, uncontrolled stimulation of non-target sides is reduced by means of distribution over multiple electrodes [27,63]. The mathematical maximum principle [31] shows that highest current amplitudes in tDCS are always in the brain areas under the stimulation electrodes. Distribution of injection current of fixed total strength

Table 3

The following table shows the interaction effect between the tDCS conditions for time courses after tDCS (Post1, Post2 and Post3) compared to control baseline time course before tDCS (Pre). Column 2 (Pre vs Post1), column 3 (Pre vs Post2) and column 3 (Pre vs Post3) shows the statistical results correspondingly, when conditions are compared, with degrees of freedom (df), F values (F) and P-values (P) (*P < 0.05, **P < 0.01, ***P < 0.001).

Conditions comparison	Pre vs Post1 (Condition x Time) df, F, P, Error(df)	Pre vs Post2 (Condition x Time) df, F, P, Error(df)	Pre vs Post3 (Condition x Time) df,F, P, Error(df)
D-CMI vs SB	1, 23.82, < **.001***, 9	1, 4.29, 0.068, 9	1, 0.899, 0.368, 9
D-CMI vs Sham	1, 10.86, **0.009**, 9	1, 0.38, 0.55, 9	1, 1.85, 0.092, 9
SB vs Sham	1, 0.526, 0.487, 9	1, 0.043, 0.840, 9	1, 1.218, 0.298, 9

over more electrodes thus means that these uncontrolled side-effects are reduced. The constrained maximum intensity (CMI) algorithm of [65] introduces a maximum injection current per-electrode to the maximum intensity (MI) algorithm proposed by Ref. [16]. CMI thus already helps considerably reducing uncontrolled side effects. When compared to CMI, the regularization in our D-CMI algorithm [27,63] further distributes the injection currents over multiple electrodes without losing a considerable amount of DIR at the target side, which is thus further reducing uncontrolled side effects. Additionally, it was shown by Ref. [63], that due to the fact that the regularization adds convexity to the optimization cost function the D-CMI solution is unique and there are no jumps of injection currents between electrodes due to for example tiny changes in volume conduction modeling or sensor registration, in contrast to CMI.

Our main experimental result, in the group of 10 subjects, supports our main hypothesis from FEM-based computer simulations: For D-CMI, 5–15 min (Post1) after stimulation, a significantly increased SEF M20, both in source space (Figs. 4 and 5, Tables 1–4) and sensor signal space (Fig. 6), is observed (Pre vs Post1), while no significant change is seen for the SB and Sham stimulations for Pre vs Post1 (Figs. 4 and 5, Tables 1–4).

In previous studies, *in vitro* and *in vivo* recordings reported subthreshold modulation of neuronal activity that was induced by electric fields with peak intensities of 0.2–0.5 V/m (approx. 0.066–0.165 A/m^2) [64,65]. In our simulations, the D-CMI approach reached directional current densities at the P20/N20 dipole target of 0.126 ± 0.070 A/m^2 (mean ± SD over subjects) in line with other modeling results [16,24,25], while SB remained at only 0.085 ± 0.044 A/m^2 (Fig. 3(b)). Our result that the DIR simulations are matching the experimental effect size thus support the hypothesis that simulated DIR can be used as a guide for planning of better controlled tDCS experiments.

The lack of a significant SB effect can have various reasons. It is first of all important to consider that Brodmann area 3b is a mainly tangentially-oriented target at the depths of the central sulcus, so that the voltage gradient along the pyramidal cells, i.e., the DIR, is rather small for SB. Our result is in agreement with [7], where SB stimulation with a rectangular patch electrode placed over M1 could not achieve a significant effect on the P20/N20 SEP component. On the other side [11], showed no significant difference in

effect size between positioning of the SB anode over either M1 or S1 with regard to the M20 SEF component. One important difference to our study at hand is that [7,11] only used 1 mA, while we used 2 mA stimulation intensity. Even more importantly, when considering the more posterior anodes in our successful D-CMI montages (see Fig. 3(a) and Suppl. Fig.2), both SB anode positioning over M1 and also S1 might be too frontal for an optimal DIR at the tangentially-oriented and deep S1 target. This has also been shown by Ref. [16] that in case of a tangential target, the placement of an SB pad over the target region misses the point of maximal stimulation, which lies between electrodes and not directly under the pad as commonly assumed.

In [5], 32 stimulation electrodes were used, from which 16 were placed over the parietal scalp (somatosensory cortex) and another 16 over the contralateral forehead. Their stimulation was thus comparable to an SB montage, too. While in Ref. [5], anodal stimulation with a total injected current of 1 mA did not produce a significant effect on the P20/N20 SEP component, the mean amplitude of the P20/N20 SEP component did increase in four of the 10 min blocks after stimulation. The reasons for the missing significance might be the same as given for our SB montage above. Interestingly though in Ref. [6], a significantly increased effect was observed for the P20/N20 SEP component after anodal tDCS when the anodal patch of 18 cm^2 was placed over the motor association cortex, including the supplementary motor area (SMA) and the dorsal premotor cortex (PMd). In their study a total injected current of 1 mA and a stimulation duration of 15 min was applied. The results indicated opposite effects on M1 and S1, i.e., M1 was inhibited, whereas S1 was excited by activation of PMd and SMA after anodal tDCS. Their study thus supports the hypothesis that areas 1 and 2, located in the postcentral gyrus, might also be involved in the modulations of S1 and might be directly affected by anodal tDCS applied over S1, as also discussed by Refs. [5,10]. This might also have been the case in our study for both the D-CMI and SB montages. However, our SB approach did not lead to the same results as presented by Ref. [6] even though our anodal electrode (35 cm^2) was placed at the C3 electrode, i.e., over M1, and we stimulated with the higher intensity of 2 mA for 10 min.

In contrast to the above-mentioned tDCS studies, in the present study, we used individually targeted and D-CMI optimized mc-tDCS montages. For the targeting, we reconstructed the P20/N20 source activity from combined SEP/SEF data in calibrated head models with regard to not only individual location, but especially individual orientation. We showed that especially target orientation has large inter-subject variability (Fig. 3(a) and Suppl. Fig.2). The D-CMI approach then produced optimized mc-tDCS montages according to both location and orientation of each subject's target in S1. We showed that this complex and individualized procedure resulted in a significantly increased effect, in our case the M20 peak signal and underlying source strength, after stimulation (Pre vs Post1, N = 10). In contrast, the SB approach did not show a significant effect on the M20 SEF peak (Pre vs Post1) even though the same total injected current of 2 mA as in D-CMI was used. The comparison of the results between D-CMI and SB approaches therefore suggests that not

Table 4

For the 10 subjects, M20 source waveform peak amplitude results are shown for post hoc paired-samples *t*-test and Cohen's d effect size for the *t*-test statistical comparisons separately for the conditions D-CMI, SB and Sham between time courses before tDCS (Pre), as control values, and after tDCS (Post), as Pre vs Post1, Pre vs Post2 and Pre vs Post3. (*P < 0.05, **P < 0.01,***P < 0.001)(d = 0.2 (Small effect), 0.5 (Medium effect), 0.8 (Large effect), 1.2 (Very large), 2 (huge)).

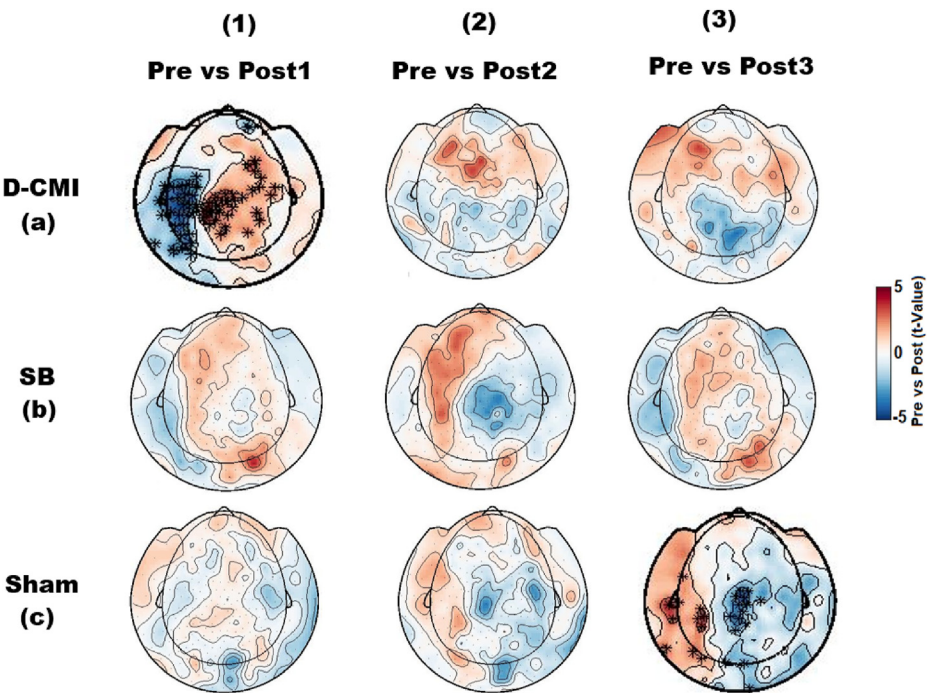| Paired *t*-testComparison	D-CMI P, effect size	SB P, effect size	Sham P, effect size
Pre vs Post1	**0.018**, 1.21	0.51, 0.74	0.85, 0.84
Pre vs Post2	0.516, 0.87	0.127, 0.56	0.146,0.81
Pre vs Post3	0.49, 0.89	0.06, 0.65	**0.031**,0.98

Fig. 6. T-value topography differences (N = 10) resulting from a comparison of the M20 (range 19–21 ms) somatosensory evoked fields (SEF) component before and after tDCS with the non-parametric cluster based permutation *t*-test. Negative (blue) and positive (red) T-value differences are shown between time courses in columns (1) Pre vs Post1 (2) Pre vs Post2 (3) Pre vs Post3 for conditions in rows (a) distributed constrained maximum intensity (D-CMI) (b) standard bipolar (SB) and (c) D-CMI sham (Sham), separately. MEG sensors showing significant differences between conditions and time courses in the non-parametric test after randomization are marked by a cross. (*P < 0.05). (For interpretation of the references to colour in this figure legend, the reader is referred to the Web version of this article.)

only individual target location, but especially individual target orientation plays an important role as also investigated and proposed by Refs. [16,18,26,28–30,32] and recently also found in a tACS study over the somatosensory cortex [33]. A total stimulation current of 2 mA might also be important, as it was earlier assumed that due to the depth of the central sulcus not enough currents reach the target area Brodmann area 3b with 1 mA [7,11].

Bipolar montages are not necessarily less effective than mc-tDCS montages, since they can also be individually optimized for intensity. It is for example well known that maximum intensity optimization for a single tangential target source leads to two electrodes that take the target in the center [16] and, as [66,67] have shown, due to Helmholtz reciprocity with the anode at the trough of the negative surface potential pole (for the somatosensory P20/N20 component the occipital trough of the N20) and the cathode at the peak of the positive surface potential pole (for the somatosensory P20/N20 component the frontal peak of the P20). D-CMI retains this basic idea, but distributes the current over several electrodes around these two main electrodes, the farther the surface pole is from the target source, the more the current is distributed without much loss of directionality (see Figs. 1 and 3(a)

and Suppl. Fig.2). Therefore, an optimized bipolar montage for a single tangential target source could thus possibly have achieved a similar effect, if the pads were centered around the two main electrodes and if the pads were cut to a size according to the size of the anodal and cathodal electrode surface areas of the D-CMI result. However, in contrast to SB, D-CMI in combination with detailed head models allows different current strengths at each single electrode to take into account idiosyncrasies in human head anatomy underlying the electrodes such as locally different injected currents due to underlying skull sutures or locally differing thicknesses of skull compacta and spongiosa. Furthermore, not only factors such as pad electrode position, shape and size influence field distributions in the brain, but also electrode–skin contact impedance and electrode shunting effects [68,69] and geled electrodes are easier to control than saline-soaked sponges. Because it was used by others [7,11] and due to practicality, we therefore decided to use the standard bipolar (SB) montage for our comparison here instead of individually-optimized bipolar montages. It might, however, be interesting in a future investigation to compare the effect size of individually optimized bipolar verses D-CMI to

Table 5
Group comparisons on intensity of perceived sensations (Itching, Pain, Burning and Warmth/Heat) separately among the conditions (D-CMI, SB and Sham) with a non-parametric Friedman ANOVA test from the questionnaire of sensations related to transcranial electrical stimulation **(1)**. Mean and standard deviation (Mean (SD)) of the scaled data are shown for the three conditions (D-CMI, SB and Sham) and each perceived sensation (Itching, Pain, Burning and Warmth/Heat) separately.

Sensations (N = 13)	D-CMI (Mean(SD))	SB (Mean(SD))	Sham (Mean(SD))	χ^2, df, P
Itching	2.08(0.76)	1.85(0.80)	1.69(0.75)	3.16, 2, 0.21
Pain	1.69(0.75)	1.31(0.48)	1.23(0.44)	4.46, 2, 0.11
Burning	1.85(0.98)	1.46(0.48)	1.69(0.51)	4.33, 2, 0.12
Warmth/Heat	1.62(0.65)	1.54(0.66)	1.23(0.43)	3.25, 2, 0.19

Degree of intensity measured according to the following scale: 1 = none, 2 = mild, 3 = moderate, and 4 = strong (standard deviations in parenthesis). Chi-square (χ^2), degrees of freedom (df),P values (P). Group differences were tested with non-parametric Friedmann test.

Table 6
We show the judgment of perceived stimulation as real (1) or sham (2) among the subjects for each condition (D-CMI, SB and Sham) separately.

Sensations	D-CMI (N = 13)	SB (N = 13)	Sham (N = 13)
Real	10	7	10
Sham	0	6	0
I don't know	3	0	3

find out if the more expensive hardware and rather large amount of work for D-CMI optimization then still pays off.

While the study in Ref. [7] showed a long-lasting increase in amplitude of EEG somatosensory components after 1 mA anodal tDCS following median nerve stimulation, the situation is more complex in our evaluation. In our later time course comparison of Pre vs Post2 and Pre vs Post3, the D-CMI and SB approach showed no significant changes on the peak amplitude of the MEG M20 source waveform, while Sham showed a significant decrease for Pre vs Post3 comparision (Table 4). Fig. 5 shows even a continuous decrease in source amplitude over time from Post1 down to Post3 for all three stimulation conditions. Similarly to our study, in Ref. [5], the time course changes in EEG N20 amplitude, evoked by stimulation of the contralateral median nerve, of their Pre vs Post2 and Pre vs Post3 decreased when compared to their Pre vs Post1 in their post-anodal 1 mA tDCS. We hypothesize that a decrease of the source amplitude over time might be due to (i) fatigue of the subjects, (ii) changes in contact impedance of the electrodes for electric finger stimulation, as well as (iii) in our case for MEG the increase in distance of the upper part of the head to the MEG dewar (and in case of EEG an electrode-skin contact impedance change and electrode shunting effects [68–70]). The latter happens especially in sitting position, but also in lying position (as in our study), resulting in registration errors, decreasing signal-to-noise ratio and thereby decreasing source amplitudes. This might then also explain why we no longer see a significant effect of D-CMI in the two later time course comparisons, where a possible increase in source amplitude might have been counter balanced by the above aspects.

While a recent study recommended an active-sham condition [71], we used here a mc-tDCS sham condition (Sham), which was based on montages created by the D-CMI approach (Fig. 2). The results showed no significant differences in sensation perceptions between the stimulation conditions (Table 5). Table 6 shows that 10 subjects considered both D-CMI and Sham to be real stimulations, while 3 subjects were unsure. SB was the only condition rated as sham by a larger subgroup (6 times as sham and 7 times as real, see Table 6), possibly just due to the change of stimulation electrodes between geled D-CMI/Sham electrodes and larger saline-solution soaked SB sponges which were just perceived as the most obvious change between the three conditions for the 6 subjects. This supports the hypothesis that our (D-CMI based) Sham condition was effective. Furthermore, our D-CMI eases sham conditioning: As D-CMI limits the maximum current per electrode and further distributes the injected currents over multiple electrodes especially at distant sides to the target, it reduces skin sensations that can occur beneath the electrodes and thereby the contrast between the D-CMI and Sham conditions.

Let us shed light on our assumption that the main effect of the P20/N20 targeted tDCS can be read out by means of our M20 pre and post-stimulation investigations in the D-CMI and SB sessions. In Ref. [8], the cortical excitability shifts by tDCS in humans was investigated. They used pharmacological modulations and found that cortical excitability shifts induced during tDCS depend on membrane polarization, thus modulating the conductance of sodium and calcium channels. More importantly for our experimental setup, they suggested that the after-effects in post-stimulation

measurements may be NMDA receptor dependent. It was, concluded that since NMDA receptors are involved in neuroplastic changes, tDCS could be successfully applied in the modulation or induction of these processes. It was also found that carbamazepine selectively eliminated the tDCS-driven excitability enhancements after tDCS (and also during tDCS). Due to these neurophysiological reasons, we can expect our main effect on the Brodmann area 3b dipole source itself. Since it is mainly tangentially oriented, the MEG is especially sensitive to changes in amplitude, so an appropriate method to read out the stimulation effects. Our experimental results support these findings and hypotheses.

We therefore also did not investigate effects of the stimulation on later components such as the P22 or the N30. This has various reasons and in short, our goal was to control our experiment as good as possible. (1) First of all, a combined EEG/MEG instead of only MEG would have allowed us to also read out effects of the stimulation on later and more radially-oriented somatosensory components. However, this was not practicable with our hardware. MEG alone is nearly blind to radial sources and thus not capable of reading out stimulation effects on the P22, as also discussed by Ref. [11]. (2) Secondly, both the P22 and N30 have different origins with regard to both location and orientation than the P20. While the P22 from area 1 originates from the crown of the gyrus and is radially oriented [49,72,73], recent investigations point to a whole network of sources that contribute to the N30 [74], namely Brodmann areas 3b and 1, the left ventrolateral thalamus and even frontal areas. Even more importantly, since the N30 topography shows in most subjects an inverted polarity to the P20, the orientation of the main contributor in Brodmann area 3b is inverted, too (Fig. 4 in Ref. [74]). (3) Thirdly, similar to (constrained) maximum intensity (MI) optimization [16,67], the D-CMI method used in this study was selected as a mainly intensity-based mc-tDCS with the goal of high directionality at the P20 target side. Due to the distribution of currents especially at distant electrodes from the target, diffused side effects as well as less sensations at the skin level such as tingling or pain are expected. On the focality-intensity scale [16,66], D-CMI is thus positioned close to MI, but slightly more focal. In contrast, focality-based optimization methods reach much lower intensity at non-target sides and thereby reduced side-effects, but at the cost of much lower directionality at the target side [16,27,31]. Therefore, due to the larger side-effects of the intensity-optimized D-CMI, the non-target P22 and N30 sources may have been stimulated by uncontrolled direct effects mixed with the incoming indirect effects from the P20 target. Due to the polarity-inverted N30 topography compared to the P20, the possibly stronger excitatory indirect effects coming in from the facilitated P20 might have thus mixed up with the inhibitory direct stimulation effects of the main N30 source in Brodmann area 3b, leading possibly to an overall effect cancellation. (4) While the P20 is an exogenous component that can even be elicited under anesthesia [13,14,36], the influence of attention and the basal state of the brain on later components increases. Also the effects of tDCS might depend on the basal state of the brain at the time of its application [75,76]. Although we tried to maintain a constant brain state in all subjects, their thoughts or expectations before, during and after the stimulation was not be controlled.

Finally, we would like to discuss a main limitation of our study. We had to reject 3 out of 13 subjects for the interaction statistics as described in Section 2.5. This might be a disadvantage of finger compared to wrist stimulation, but because of the higher level of sensation, we feared losing too many subjects with electric wrist stimulation, especially due to the many sessions and runs.

In our future work one focus will be on clinical applications, for example with the goal to reduce epileptic activity in focal epilepsy, where the large potential of tDCS has recently been shown [77,78].

A first proof-of-principle investigation of our EEG/MEG targeted and D-CMI optimized mc-tDCS approach also showed already very promising results [79,80]. An interesting further experiment would also be to compare effects of targeted and optimized mc-tDCS with effects of targeted and optimized bipolar montages (in contrast to the standard bipolar montages that we used here). Such studies are necessary to determine the contribution but also limits of multi-channel tDCS hardware.

5. Conclusion

In conclusion, this first application of our EEG/MEG targeted and D-CMI optimized mc-tDCS approach in a single blinded, sham-controlled somatosensory experiment showed a significant, though short-lasting stimulation effect on the P20/N20 source activity in Brodmann area 3b, while this could not be achieved with standard bipolar stimulation. MEG was successfully used to sensitively read out stimulation effects on the more tangentially-oriented lateral target sources in S1. Accurate targeting was performed using combined EEG/MEG in realistic skull-conductivity-calibrated finite element method head models. Our individualized targeting and stimulation approach might thus help to better control tDCS experimental paradigms. Our approach is also interesting for tACS, where recent studies also showed that neuro-imaging combined with electric field modeling is useful to explain inter-individual variability of stimulation effects [15,33].

CRediT authorship contribution statement

Asad Khan: Data curation, Software, Methodology, Formal analysis, Investigation, Conceptualization, Visualization, Validation, Writing − original draft. **Marios Antonakakis:** Writing − review & editing, Software. **Sonja Suntrup-Krueger:** Conceptualization, Writing − review & editing. **Rebekka Lencer:** Conceptualization, Writing − review & editing. **Michael A. Nitsche:** Conceptualization, Writing − review & editing. **Walter Paulus:** Conceptualization, Writing − review & editing. **Joachim Groß:** Writing − review & editing, Resources. **Carsten H. Wolters:** Conceptualization, Supervision, Funding acquisition, Project administration, Validation, Software, Resources, Methodology, Writing − review & editing.

Declaration of competing interest

The authors declare that they have no known competing financial interests or personal relationships that could have appeared to influence the work reported in this paper.

Acknowledgements

Appendix A. Supplementary data

Supplementary data to this article can be found online at https://doi.org/10.1016/j.brs.2022.12.006.

References

[1] Antal A, Alekseichuk I, Bikson M, Brockmöller J, Brunoni AR, Chen R, et al. Low intensity transcranial electric stimulation: safety, ethical, legal regulatory and application guidelines. Clin Neurophysiol 2017. https://doi.org/10.1016/j.clinph.2017.06.001.

[2] Lefaucheur J-P. A comprehensive database of published tDCS clinical trials (20052016). Neurophysiol Clin Neurophysiol 2016;46:319–98. https://doi.org/10.1016/j.neucli.2016.10.002.

[3] Nitsche MA, Cohen LG, Wassermann EM, Priori A, Lang N, Antal A, et al. Transcranial direct current stimulation: state of the art 2008. Brain Stimul 2008;1:206–23. https://doi.org/10.1016/j.brs.2008.06.004.

[4] Schutter DJLG, Wischnewski M. A meta-analytic study of exogenous oscillatory electric potentials in neuroenhancement. Neuropsychologia 2016;86:110–8. https://doi.org/10.1016/j.neuropsychologia.2016.04.011.

[5] Dieckhöfer A, Waberski TD, Nitsche M, Paulus W, Buchner H, Gobbelé R. Transcranial direct current stimulation applied over the somatosensory cortex - differential effect on low and high frequency SEPs. Clin Neurophysiol 2006;117:2221–7. https://doi.org/10.1016/j.clinph.2006.07.136.

[6] Kirimoto H, Ogata K, Onishi H, Oyama M, Goto Y, Tobimatsu S. Transcranial direct current stimulation over the motor association cortex induces plastic changes in ipsilateral primary motor and somatosensory cortices. Clin Neurophysiol Off J Int Fed Clin Neurophysiol 2011;122:777–83. https://doi.org/10.1016/j.clinph.2010.09.025.

[7] Matsunaga K, Nitsche MA, Tsuji S, Rothwell JC. Effect of transcranial DC sensorimotor cortex stimulation on somatosensory evoked potentials in humans. Clin Neurophysiol 2004;115:456–60. https://doi.org/10.1016/s1388-2457(03)00362-6.

[8] Nitsche MA, Nitsche MS, Klein CC, Tergau F, Rothwell JC, Paulus W. Level of action of cathodal DC polarisation induced inhibition of the human motor cortex. Clin Neurophysiol 2003;114:600–4. https://doi.org/10.1016/S1388-2457(02)00412-1.

[9] Nitsche MA, Paulus W. Excitability changes induced in the human motor cortex by weak transcranial direct current stimulation. J Physiol 2000;527:633–9. https://doi.org/10.1111/j.1469-7793.2000.t01-1-00633.x.

[10] Sehm B, Hoff M, Gundlach C, Taubert M, Conde V, Villringer A, et al. A novel ring electrode setup for the recording of somatosensory evoked potentials during transcranial direct current stimulation (tDCS). J Neurosci Methods 2013;212:234–6.

[11] Sugawara K, Onishi H, Yamashiro K, Kojima S, Miyaguchi S, Kirimoto H, et al. The effect of anodal transcranial direct current stimulation over the primary motor or somatosensory cortices on somatosensory evoked magnetic fields. Clin Neurophysiol 2015;126:60–7. https://doi.org/10.1016/j.clinph.2014.04.014.

[12] Allison T, Mccarthy G, Wood CC, Jones SJ. Potentials evoked in human and monkey cerebral cortex by stimulation of the median nerve. Brain 1991;114:2465–503. https://doi.org/10.1093/brain/114.6.2465.

[13] Buchner H, Fuchs M, Wischmann HA, Dössel O, Ludwig I, Knepper A, et al. Source analysis of median nerve and finger stimulated somatosensory evoked potentials: multichannel simultaneous recording of electric and magnetic fields combined with 3d-MR tomography. Brain Topogr 1994;6:299–310. https://doi.org/10.1007/BF01211175.

[14] Hari R, Puce A. MEG-EEG primer. Oxford University Press; 2017. https://doi.org/10.1093/med/9780190497774.001.0001.

[15] Kasten FH, Duecker K, Maack MC, Meiser A, Herrmann CS. Integrating electric field modeling and neuroimaging to explain inter-individual variability of {tACS} effects. Nat Commun 2019;10. https://doi.org/10.1038/s41467-019-13417-6.

[16] Dmochowski JP, Datta A, Bikson M, Su Y, Parra LC. Optimized multi-electrode stimulation increases focality and intensity at target. J Neural Eng 2011;8(4):046011. https://doi.org/10.1088/1741-2560/8/4/046011.

[17] Veniero D, Benwell CSY, Ahrens MM, Thut G. Inconsistent effects of parietal α-tACS on pseudoneglect across two experiments: a failed internal replication. Front Psychol 2017;8. https://doi.org/10.3389/fpsyg.2017.00952.

[18] Evans C, Zich C, Lee JSA, Ward N, Bestmann S. Inter-individual variability in current direction for common tDCS montages. Neuroimage 2022;260:119501. https://doi.org/10.1016/j.neuroimage.2022.119501. 10.1016/j.neuroimage.2022.119501.

[19] Laakso I, Tanaka S, Koyama S, Santis V De, Hirata A. Inter-subject variability in electric fields of motor cortical tDCS. Brain Stimul 2015;8:906–13. https://doi.org/10.1016/j.brs.2015.05.002.

[20] López-Alonso V, Cheeran B, R\'\io-Rodr\'\iguez D, Fernández-del-Olmo M. Inter-individual variability in response to non-invasive brain stimulation paradigms. Brain Stimul 2014;7:372–80. https://doi.org/10.1016/j.brs.2014.02.004.

[21] Antonakakis M, Schrader S, Aydin Ü, Khan A, Gross J, Zervakis M, et al. Inter-subject variability of skull conductivity and thickness in calibrated realistic head models. Neuroimage 2020;223:117353. https://doi.org/10.1016/j.neuroimage.2020.117353.

[22] Antonakakis M, Schrader S, Wollbrink A, Oostenveld R, Rampp S, Haueisen J, et al. The effect of stimulation type, head modeling, and combined EEG and MEG on the source reconstruction of the somatosensory P20/N20 component. Hum Brain Mapp 2019;40:5011–28. https://doi.org/10.1002/hbm.24754.

[23] Huang Y, Liu A, Lafon B, Friedman D, Dayan M, Wang X, et al. Measurements and models of electric fields in the in vivo human brain during transcranial electric stimulation. Brain Stimul 2017;10:e25–6. https://doi.org/10.1016/j.brs.2017.04.022.

[24] Opitz A, Paulus W, Will S, Antunes A, Thielscher A. Determinants of the electric field during transcranial direct current stimulation. Neuroimage 2015;109:140–50. https://doi.org/10.1016/j.neuroimage.2015.01.033.

[25] Wagner S, Rampersad SM, Aydin Ü, Vorwerk J, Oostendorp TF, Neuling T, et al. Investigation of tDCS volume conduction effects in a highly realistic head model. J Neural Eng 2014;11. https://doi.org/10.1088/1741-2560/11/1/016002. 16002.

[26] Creutzfeldt OD, Fromm GH, Kapp H. Influence of transcortical d-c currents on cortical neuronal activity. Exp Neurol 1962;5:436–52. https://doi.org/10.1016/0014-4886(62)90056-0.

[27] Khan A, Antonakakis M, Vogenauer N, Haueisen J, Wolters CH. Individually optimized multi-channel tDCS for targeting somatosensory cortex. Clin Neurophysiol 2022;134:9–26. https://doi.org/10.1016/j.clinph.2021.10.016.

[28] Krieg TD, Salinas FS, Narayana S, Fox PT, Mogul DJ. PET-based confirmation of orientation sensitivity of TMS-induced cortical activation in humans. Brain Stimul 2013;6:898–904. https://doi.org/10.1016/j.brs.2013.05.007.

[29] Krieg TD, Salinas FS, Narayana S, Fox PT, Mogul DJ. Computational and experimental analysis of TMS-induced electric field vectors critical to neuronal activation. J Neural Eng 2015;12:46014. https://doi.org/10.1088/1741-2560/12/4/046014.

[30] Seo H, Jun SC. Multi-scale computational models for electrical brain stimulation. Front Hum Neurosci 2017;11. https://doi.org/10.3389/fnhum.2017.00515.

[31] Wagner S, Burger M, Wolters CH. An optimization approach for well-targeted transcranial direct current stimulation. SIAM J Appl Math 2016;76:2154–74. https://doi.org/10.1137/15m1026481.

[32] Radman T, Ramos RL, Brumberg JC, Bikson M. Role of cortical cell type and morphology in subthreshold and suprathreshold uniform electric field stimulation in vitro. Brain Stimul 2009;2:215–28. https://doi.org/10.1016/j.brs.2009.03.007. e3.

[33] Mohd Zulkifly MF, Lehr A, van de Velden D, Khan A, Focke NK, Wolters CH, et al. Directionality of the injected current targeting the P20/N20 source determines the efficacy of 140 Hz transcranial alternating current stimulation (tACS)-induced aftereffects in the somatosensory cortex. PLoS One 2022;17:1–24. https://doi.org/10.1371/journal.pone.0266107.

[34] Desmedt JE, Tomberg C. Mapping early somatosensory evoked potentials in selective attention: critical evaluation of control conditions used for titrating by difference the cognitive P30, P40, P100 and N140. Electroencephalogr Clin Neurophysiol Evoked Potentials 1989;74:321–46. https://doi.org/10.1016/0168-5597(89)90001-4.

[35] Josiassen RC, Shagass C, Roemer RA, Slepner S, Czartorysky B. Early cognitive components of somatosensory event-related potentials. Int J Psychophysiol 1990;9:139–49. https://doi.org/10.1016/0167-8760(90)90068-O.

[36] Jäntti V, Sonkajärvi E, Mustola S, Rytky S, Kiiski P, Suominen K. Single-sweep cortical somatosensory evoked potentials: N20 and evoked bursts in sevoflurane anaesthesia. Electroencephalogr Clin Neurophysiol Potentials Sect 1998;108:320–4. https://doi.org/10.1016/S0168-5597(98)00005-7.

[37] Ruthotto L, Kugel H, Olesch J, Fischer B, Modersitzki J, Burger M, et al. Diffeomorphic susceptibility artifact correction of diffusion-weighted magnetic resonance images. Phys Med Biol 2012;57:5715–31. https://doi.org/10.1088/0031-9155/57/18/5715.

[38] Rice JK, Rorden C, Little JS, Parra LC. Subject position affects EEG magnitudes. Neuroimage 2013;64:476–84. https://doi.org/10.1016/j.neuroimage.2012.09.041.

[39] Sarvas J. Basic mathematical and electromagnetic concepts of the biomagnetic inverse problem. Phys Med Biol 1987;32(1):11–22. https://doi.org/10.1088/0031-9155/32/1/004.

[40] Gross J, Junghöfer M, Wolters CH. Bioelectromagnetism in human brain research: new applications, new questions. The Neuroscientist; 2021. https://doi.org/10.1177/10738584211054742.

[41] Huang M-X, Song T, Hagler DJ, Podgorny I, Jousmaki V, Cui L, et al. A novel integrated MEG and EEG analysis method for dipolar sources. Neuroimage 2007;37:731–48. https://doi.org/10.1016/j.neuroimage.2007.06.002.

[42] Dassios G, Fokas AS, Hadjiloizi D. On the complementarity of electroencephalography and magnetoencephalography. Inverse Probl 2007;23:2541–9. https://doi.org/10.1088/0266-5611/23/6/016.

[43] Vorwerk J, Aydin Ü, Wolters CH, Butson CR. Influence of head tissue conductivity uncertainties on EEG dipole reconstruction. Front Neurosci 2019;13. https://doi.org/10.3389/fnins.2019.00531.

[44] Jenkinson M, Beckmann CF, Behrens TEJ, Woolrich MW, Smith SM. FSL. Neuroimage 2012;62:782–90. https://doi.org/10.1016/j.neuroimage.2011.09.015.

[45] Lanfer B, Scherg M, Dannhauer M, Knösche TR, Burger M, Wolters CH. Influences of skull segmentation inaccuracies on EEG source analysis. Neuroimage 2012;62:418–31. https://doi.org/10.1016/j.neuroimage.2012.05.006.

[46] Wolters CH, Anwander A, Berti G, Hartmann U. Geometry-adapted hexahedral meshes improve accuracy of finite-element-method-based EEG source analysis. IEEE Trans Biomed Eng 2007;54:1446–53. https://doi.org/10.1109/tbme.2007.890736.

[47] Ramon C, Schimpf P, Haueisen J, Holmes M, Ishimaru A. Role of soft bone, CSF and gray matter in EEG simulations. Brain Topogr 2004;16:245–8. https://doi.org/10.1023/B:BRAT.0000032859.68959.76.

[48] Baumann SB, Wozny DR, Kelly SK, Meno FM. The electrical conductivity of human cerebrospinal fluid at body temperature. IEEE Trans Biomed Eng 1997;44:220–3. https://doi.org/10.1109/10.554770.

[49] Fuchs M, Wagner M, Wischmann H-A, Köhler T, Theißen A, Drenckhahn R, et al. Improving source reconstructions by combining bioelectric and biomagnetic data. Electroencephalogr Clin Neurophysiol 1998;107:93–111. https://doi.org/10.1016/s0013-4694(98)00046-7.

[50] Rullmann M, Anwander A, Dannhauer M, Warfield S, Duffy F, Wolters C. EEG source analysis of epileptiform activity using a 1~mm anisotropic hexahedra finite element head model. Neuroimage 2009;44:399–410. https://doi.org/10.1016/j.neuroimage.2008.09.009.

[51] Vorwerk J, Cho J-H, Rampp S, Hamer H, Knösche TR, Wolters CH. A guideline for head volume conductor modeling in EEG and MEG. Neuroimage 2014;100:590–607. https://doi.org/10.1016/j.neuroimage.2014.06.040.

[52] Medani T, Lautru D, Schwartz D, Ren Z, Sou G. FEM method for the EEG forward problem and improvement based on modification of the saint venant's method. Prog Electromagn Res 2015;153:11–22. https://doi.org/10.2528/pier15050102.

[53] Wolters CH, Grasedyck L, Hackbusch W. Efficient computation of lead field bases and influence matrix for the FEM-based EEG and MEG inverse problem. Inverse Probl 2004;20:1099–116. https://doi.org/10.1088/0266-5611/20/4/007.

[54] Lew S, Wolters CH, Dierkes T, Röer C, MacLeod RS. Accuracy and run-time comparison for different potential approaches and iterative solvers in finite element method based EEG source analysis. Appl Numer Math 2009;59. https://doi.org/10.1016/j.apnum.2009.02.006. 1970–88.

[55] Wolters CH, Kuhn M, Anwander A, Reitzinger S. A parallel algebraic multigrid solver for finite element method based source localization in the human brain. Comput Visual Sci 2002;5:165–77. https://doi.org/10.1007/s00791-002-0098-0.

[56] Schrader S, Antonakakis M, Rampp S, Engwer C, Wolters CH. A novel method for calibrating head models to account for variability in conductivity and its evaluation in a sphere model. Phys Med Biol 2020;65:245043. https://doi.org/10.1088/1361-6560/abc5aa.

[57] Akhtari M, Bryant HC, Mamelak AN, Flynn ER, Heller L, Shih JJ, Mandelkern M, Matlachov A, Ranken DM, Best ED, DiMauro MA, Lee RR, Sutherling WW. Conductivities of three-layer human skull. Brain Topogr 2002;14(3):151–67. https://doi.org/10.1023/A:1007882102297.

[58] Wolters CH, Beckmann RF, Rienäcker A, Buchner H. No title. Brain Topogr 1999;12:3–18. https://doi.org/10.1023/a:1022281005608.

[59] Oostenveld R, Fries P, Maris E, Schoffelen J-M. FieldTrip: open source software for advanced analysis of MEG, EEG, and invasive electrophysiological data. Comput Intell Neurosci 2011;2011:156869. https://doi.org/10.1155/2011/156869.

[60] Nakamura A, Yamada T, Goto A, Kato T, Ito K, Abe Y, et al. Somatosensory homunculus as drawn by MEG. Neuroimage 1998;7:377–86. https://doi.org/10.1006/nimg.1998.0332.

[61] Aydin Ü, Rampp S, Wollbrink A, Kugel H, Cho J-H, Knösche TR, et al. Zoomed MRIGuided by combined EEG/MEG source analysis: a multimodal approach forOptimizing presurgical epilepsy work-up and its application in a multifocalEpilepsy patient case study. Brain Topogr 2017;30(4):417–33. https://doi.org/10.1007/s10548-017-0568-9.

[62] Antonakakis M, Schrader S, Aydin Ü, Khan A, Gross J, Zervakis M, et al. InterSubjectVariability of skull conductivity and thickness in calibrated realistic HeadModels. Neuroimage 2020;223:117353. https://doi.org/10.1016/j.neuroimage.2020.117353.

[63] Frank A. Master thesis in mathematics. University of Münster; 2022. http://www.sci.utah.edu/~wolters/PaperWolters/2022/MasterFrank.pdf.

[64] Francis JT, Gluckman BJ, Schiff SJ. Sensitivity of neurons to weak electric fields. J Neurosci 2003;23:7255. https://doi.org/10.1523/JNEUROSCI.23-19-07255.2003. LP – 7261.

[65] Fröhlich F, McCormick DA. Endogenous electric fields may guide neocortical network activity. Neuron 2010;67:129–43. https://doi.org/10.1016/j.neuron.2010.06.005.

[66] Fernández-Corazza M, Turovets S, Muravchik CH. Unification of optimal targeting methods in transcranial electrical stimulation. Neuroimage 2020;209:116403. https://doi.org/10.1016/j.neuroimage.2019.116403.

[67] Guler S, Dannhauer M, Erem B, Macleod R, Tucker D, Turovets S, et al. Optimization of focality and direction in dense electrode array transcranial direct current stimulation (tDCS). J Neural Eng 2016;13. https://doi.org/10.1088/1741-2560/13/3/036020.

[68] Pursiainen S, Agsten B, Wagner S, Wolters CH. Advanced boundary electrode modeling for tES and parallel tES/EEG. IEEE Trans Neural Syst Rehabil Eng 2018;26:37–44. https://doi.org/10.1109/TNSRE.2017.2748930.

[69] Saturnino GB, Antunes A, Thielscher A. On the importance of electrode parameters for shaping electric field patterns generated by tDCS. Neuroimage 2015;120:25–35. https://doi.org/10.1016/j.neuroimage.2015.06.067.

[70] Pursiainen S, Lucka F, Wolters CH. Complete electrode model in EEG: relationship and differences to the point electrode model. Phys Med Biol 2012;57:999–1017. https://doi.org/10.1088/0031-9155/57/4/999.

[71] Neri F, Mencarelli L, Menardi A, Giovannelli F, Rossi 1096 S, Sprugnoli G, et al. A novel tDCS sham approach based on model-driven controlled shunting. Brain Stimul 2020;13:507–16. https://doi.org/10.1016/j.brs.2019.11.004.

[72] Buchner H, Waberski TD, Fuchs M, Drenckhahn R, Wagner M, Wichmann H-A. Postcentral origin of P22: evidence from source reconstruction in a realistically shaped head model and from a patient with a postcentral lesion. Electroencephalogr Clin Neurophysiol Potentials Sect 1996;100:332–42. https://doi.org/10.1016/0168-5597(96)95678-6.

[73] Haueisen J, Leistritz L, Süsse T, Curio G, Witte H. Identifying mutual information transfer in the brain with differential-algebraic modeling: evidence for fast oscillatory coupling between cortical somatosensory areas 3b and 1. Neuroimage 2007;37:130–6. https://doi.org/10.1016/j.neuroimage.2007.04.036.

[74] Rezaei A, Lahtinen J, Neugebauer F, Antonakakis M, Piastra MC, Koulouri A, et al. Reconstructing subcortical and cortical somatosensory activity via the RAMUS inverse source analysis technique using median nerve SEP data. Neuroimage 2021;245:118726. https://doi.org/10.1016/j.neuroimage.2021.118726.

[75] Woods AJ, Antal A, Bikson M, Boggio PS, Brunoni AR, Celnik P, et al. A technical guide to tDCS, and related non-invasive brain stimulation tools. Clin Neurophysiol 2016;127:1031–48. https://doi.org/10.1016/j.clinph.2015.11.012.

[76] Li LM, Uehara K, Hanakawa T. The contribution of interindividual factors to variability of response in transcranial direct current stimulation studies. Front Cell Neurosci 2015;9. https://doi.org/10.3389/fncel.2015.00181.

[77] Yang D, Wang Q, Xu C, Fang F, Fan J, Li L, et al. Transcranial direct current stimulation reduces seizure frequency in patients with refractory focal epilepsy: a randomized, double-blind, sham-controlled, and three-arm parallel multicenter study. Brain Stimul 2020;13:109–16. https://doi.org/10.1016/j.brs.2019.09.006.

[78] Kaufmann E, Hordt M, Lauseker M, Palm U, Noachtar S. Acute effects of spaced cathodal transcranial direct current stimulation in drug resistant focal epilepsies. Clin Neurophysiol Off J Int Fed Clin Neurophysiol 2021;132:1444–51. https://doi.org/10.1016/j.clinph.2021.03.048.

[79] Wolters CH, Antonakakis M, Kaiser F, Rampp S, Kellinghaus C, Kovac S, Gross J, Möddel G. Combined EEG/MEG and optimized transcranial direct current stimulation for non-invasive diagnosis and therapy of focal epilepsy. In: IEEE-EMBS int. Conf. On biomedical and health informatics (BHI'22) jointly organized with the 17TH IEEE-EMBS int. Conf. On wearable and implantable body sensor networks (BSN'22), september 27-30, 2022, ioannina, Greece; 2022. http://www.sci.utah.edu/∼wolters/PaperWolters/2022/WoltersEtAl_IEEE-BHI-BSN_2022.pdf.

[80] Antonakakis M, Rampp S, Kellinghaus C, Wolters CH, Moeddel G. Individualized targeting and optimization of multi-channel transcranial direct current stimulation in drug-resistant epilepsy. In: 2019 IEEE 19th int. Conf. Bioinforma. Bioeng.; 2019. p. 871–6. https://doi.org/10.1109/BIBE.2019.00162.